JGP Journal of General Physiology

ARTICLE

Single-cell temperature mapping with fluorescent thermometer nanosheets

Kotaro Oyama[1,2,3,4*], Mizuho Gotoh[3,4*], Yuji Hosaka[1], Tomoko G. Oyama[1], Aya Kubonoya[3], Yuma Suzuki[3], Tomomi Arai[3,4], Seiichi Tsukamoto[3], Yuki Kawamura[5], Hideki Itoh[5,6], Seine A. Shintani[7], Toshiko Yamazawa[8], Mitsumasa Taguchi[1], Shin'ichi Ishiwata[9], and Norio Fukuda[3]

Recent studies using intracellular thermometers have shown that the temperature inside cultured single cells varies heterogeneously on the order of 1°C. However, the reliability of intracellular thermometry has been challenged both experimentally and theoretically because it is, in principle, exceedingly difficult to exclude the effects of nonthermal factors on the thermometers. To accurately measure cellular temperatures from outside of cells, we developed novel thermometry with fluorescent thermometer nanosheets, allowing for noninvasive global temperature mapping of cultured single cells. Various types of cells, i.e., HeLa/HEK293 cells, brown adipocytes, cardiomyocytes, and neurons, were cultured on nanosheets containing the temperature-sensitive fluorescent dye europium (III) thenoyltrifluoroacetonate trihydrate. First, we found that the difference in temperature on the nanosheet between nonexcitable HeLa/HEK293 cells and the culture medium was less than 0.2°C. The expression of mutated type 1 ryanodine receptors (R164C or Y523S) in HEK293 cells that cause Ca^{2+} leak from the endoplasmic reticulum did not change the cellular temperature greater than 0.1°C. Yet intracellular thermometry detected an increase in temperature of greater than ∼2°C at the endoplasmic reticulum in HeLa cells upon ionomycin-induced intracellular Ca^{2+} burst; global cellular temperature remained nearly constant within ±0.2°C. When rat neonatal cardiomyocytes or brown adipocytes were stimulated by a mitochondrial uncoupling reagent, the temperature was nearly unchanged within ±0.1°C. In cardiomyocytes, the temperature was stable within ±0.01°C during contractions when electrically stimulated at 2 Hz. Similarly, when rat hippocampal neurons were electrically stimulated at 0.25 Hz, the temperature was stable within ±0.03°C. The present findings with nonexcitable and excitable cells demonstrate that heat produced upon activation in single cells does not uniformly increase cellular temperature on a global basis, but merely forms a local temperature gradient on the order of ∼1°C just proximal to a heat source, such as the endoplasmic/sarcoplasmic reticulum ATPase.

Introduction

In the past two decades, fluorescent thermometer technology has dramatically advanced the measurement of cellular temperatures. These thermometers enable the detection of temperature changes/distributions in single cells by a magnitude of greater than ∼1°C (for review see, Suzuki et al., 2015a; Uchiyama et al., 2017; Okabe et al., 2018). Okabe et al. (2012), in particular, have developed a fluorescent polymeric thermometer, and showed that temperature is heterogeneously distributed within a COS7 cell on the order of 1°C. They reported that the temperature is a few degrees centigrade higher in the nuclei than in the cytoplasm, which was recently confirmed by using a fluorescent protein–based thermometer (Nakano et al., 2017). It has likewise been reported that the temperature in single living cells is higher than the culture medium by greater than ∼1°C (Okabe et al., 2012; Sekiguchi et al., 2018).

In contrast to these experimental findings, in-depth theoretical calculations by us (Takei et al., 2014) and others (Yang et al., 2011; Sato et al., 2014; Baffou et al., 2014) have provided striking evidence that the cellular temperature is unlikely to rise by greater than ∼1°C, at least under physiological conditions,

[1]Quantum Beam Science Research Directorate, National Institutes for Quantum and Radiological Science and Technology, Gunma, Japan; [2]Precursory Research for Embryonic Science and Technology, Japan Science and Technology Agency, Saitama, Japan; [3]Department of Cell Physiology, The Jikei University School of Medicine, Tokyo, Japan; [4]Department of Physics, School of Advanced Science and Engineering, Waseda University, Tokyo, Japan; [5]Department of Pure and Applied Physics, Graduate School of Advanced Science and Engineering, Waseda University, Tokyo, Japan; [6]Epithelial Biology Laboratory, Institute of Medical Biology, Agency for Science, Technology and Research, Singapore; [7]Department of Biomedical Sciences, College of Life and Health Sciences, Chubu University, Aichi, Japan; [8]Department of Molecular Physiology, The Jikei University School of Medicine, Tokyo, Japan; [9]Department of Physics, Faculty of Science and Engineering, Waseda University, Tokyo, Japan.

*K. Oyama and M. Gotoh contributed equally to this paper; Correspondence to Norio Fukuda: noriof@jikei.ac.jp; Kotaro Oyama: oyama.kotaro@qst.go.jp; Shin'ichi Ishiwata: ishiwata@waseda.jp.

© 2020 Oyama et al. This article is distributed under the terms of an Attribution–Noncommercial–Share Alike–No Mirror Sites license for the first six months after the publication date (see http://www.rupress.org/terms/). After six months it is available under a Creative Commons License (Attribution–Noncommercial–Share Alike 4.0 International license, as described at https://creativecommons.org/licenses/by-nc-sa/4.0/).

such as upon activation of Ca^{2+}-ATPase pumps in the ER/SR. These calculations predict that the heat necessary for an increase in the cell-size water is estimated to be ~10 μW, i.e., ~100,000-fold higher than that produced in a single cell (~100 pW). This "10^5 gap issue" raises the question of the reliability or accuracy of single-cell thermometry (see Suzuki et al., 2015b). A major problem regarding single-cell thermometry when performed inside living cells is that the effects of various nonthermal factors on thermometers, if any, cannot be ruled out. Therefore, experimental data need to be subsequently corrected for potential nonthermal factors, e.g., pH, ionic strength, and viscosity, obtained in a separate set of experiments (see Zohar et al., 1998; Yang et al., 2011; Okabe et al., 2012; Takei et al., 2014; Kriszt et al., 2017). In addition, high-density macromolecular assemblies consisting of cytoskeletal networks (e.g., actin filaments and microtubules), membranous organelles (e.g., Golgi apparatuses, mitochondria, and ER) and other molecules such as RNA are present at high densities inside living cells (Albe et al., 1990; Ellis, 2001; Milo, 2013). Furthermore, physical factors, such as the electrical/magnetic field inside cells, that may potentially affect thermometers remain to be investigated. Therefore, in order to clarify whether or not intracellular temperature is heterogeneously distributed, thermometry needs to be performed from outside of cells, thereby excluding unknown/unexpected effects on thermometers.

To the knowledge of the authors, we were the first to detect an increase in cellular temperature from the outside of a single cell, by using a fluorescent microthermometer (Suzuki et al., 2007), i.e., a tip of a glass microcapillary filled with the fluorescent temperature-sensitive dye europium (III) thenoyltrifluoroacetonate trihydrate (EuTTA). One advantage of this method is that the EuTTA is hardly affected by environmental nonthermal factors, because of the glass microcapillary acting as a physical barrier (Zeeb et al., 2004). We found that when the microthermometer was pressed on a single HeLa cell, an ~1°C increase in the surface temperature was detected in response to an ionophore-induced large intracellular Ca^{2+} burst (Suzuki et al., 2007); viz., a finding confirmed in follow-up studies under similar experimental conditions (Yang et al., 2011; Takei et al., 2014; Itoh et al., 2016). Further, studies by others using other types of extracellular thermometers, i.e., thermocouples (Wang et al., 2011; Yang et al., 2017), cantilevers (Sato et al., 2014), resonators (Inomata et al., 2012, 2016), and diode thermal sensors (Yamada et al., 2016), similarly reported increases in cellular temperature upon activation by a magnitude of ~0.1°C or higher. These studies appear to support the notion that living cells per se increase their temperatures at the single cell level, and may efficiently use the heat to, e.g., promote enzymatic reactions. It should, however, be noted that these point-measurement methods are unable to indicate (a) at which region of a cell the heat is produced, and (b) how the heat disperses to the cytosol as well as to various organelles.

In the present study, we developed novel thermometry with fluorescent thermometer nanosheets (thickness, ~50 nm) allowing for noninvasive cellular temperature mapping from outside of living cells. We cultured various types of cells, i.e., HeLa/HEK293 cells, cardiomyocytes, and neurons, on the nanosheet and systematically investigated whether or not the global cellular temperature is changed upon activation. The present study demonstrated that (a) the difference between the global temperature of HeLa/HEK293 cells and the medium was <0.2°C, (b) physiological excitations did not alter the global temperature in excitable cells (i.e., cardiomyocytes and neurons) by >0.03°C, and (c) while the intracellular temperature increased at the ER by >2°C during ionophore-induced cytoplasmic Ca^{2+} burst induced by Ca^{2+} in HeLa cells, the global temperature remained nearly stable within ±0.2°C. Based on these findings, the physiological implications regarding endogenous heat production in various types of cells are discussed.

Materials and methods

All experimental procedures conformed to the Guidelines for Proper Conduct of Animal Experiments approved by the Science Council of Japan and were performed in accordance with the Waseda University Guidelines for Care and Use of Laboratory Animals. Likewise, the present study protocol was approved by the Animal Care Committee of The Jikei University School of Medicine and the Animal Experiment Committee of the National Institutes for Quantum and Radiological Science and Technology.

Preparation of fluorescent thermometer nanosheets

EuTTA and ratiometric thermometer (RT) nanosheets were prepared as follows: viz., for preparation of EuTTA nanosheets, 5 mg/ml EuTTA (Acros Organics), and 10 mg/ml poly(methyl methacrylate) (PMMA; molecular weight, 15,000; Sigma-Aldrich, Merck) were dissolved in chloroform. For preparation of RT nanosheets, 5 mg/ml EuTTA, 10 mg/ml PMMA, and 2.5 μg/ml rhodamine 101 (Rh101; Santa Cruz Biotechnology) were dissolved in chloroform. A small amount of the solution (i.e., 100 μl) was dropped on a coverslip of a prewashed 35-mm culture dish (3911–035, AGC Techno Glass), and the dish was spincoated at 3,000 rpm for 10 s (MS-B100, Mikasa). The thickness and surface roughness of RT nanosheets were measured by an atomic force microscope (AFM5300E, Hitachi High-Technologies).

In experiments with cardiomyocytes, the Rh101 concentration was increased to 12.5 μg/ml to increase the frame rate (see Temperature measurement for cardiomyocytes for details). In experiments with neurons, the nanosheets were coated on polymer-bottom dishes (SF-T-D12, Fine Plus International), which were spincoated at 2,000 rpm for 10 s (MS-A100, Mikasa). The aggregates of fluorescent dyes could have been removed using a 0.2-μm filter (SYTF0301MNXX104, mdi Membrane Technologies); however, we did not do so in the present study because the aggregates were used for focus adjustment during microscopic observation.

Microscopic systems for detection of temperature sensitivity of RT nanosheets

An inverted microscope (IX-70, Olympus) was used for the detection of temperature sensitivity of RT nanosheets; an electron multiplying charge coupled device (EMCCD) camera (Luca S

DL-658M-TIL, Andor Technology) was mounted on the microscope with a 0.63× zoom lens (U-TV0.63XC, Olympus). EuTTA, Rh101, and the fluorescent Ca^{2+} indicator Fluo4 (Thermo Fisher Scientific) were excited by a four-wavelength high-power LED source (LED4D237, 365/490/565/660 nm, Thorlabs), and observed by a PlanApo N 60×/1.45 oil immersion objective lens (Olympus). The excitation light was changed using an optical filter changer Lambda 10–3 (Sutter Instrument). Excitation filters BP360–370 (Olympus) and FF01-554/23 (Semrock, IDEX Health & Science) were used for EuTTA and Rh101, respectively. A dichroic mirror FF493/574-Di01 (Semrock) and an emission filter FF01-512/630 (Semrock) were used for both cases.

A glass-bottom dish with a RT nanosheet was filled with 3 ml PBS (137 mM NaCl, 2.7 mM KCl, 1.5 mM KH_2PO_4, and 8.1 mM Na_2HPO_4). The dish was incubated on a sample stage for 15 min to stabilize the temperature at 36°C. 50 frames of fluorescence images were captured for both EuTTA and Rh101 at an exposure time of 100 ms. Background images were captured with no excitation light. The solution temperature was adjusted to 40°C by a thermostatically controlled incubator (INUG2-ONICS, Tokai Hit). After the temperature became stabilized, the focus and the position of the RT nanosheet were adjusted, and thereafter the images were captured under the same condition (procedures were repeated for each temperature measurement). The photobleaching effects were corrected by single-exponential fitting to the fluorescence intensity (F.I.) at 36°C (as in Suzuki et al., 2007; Takei et al., 2014).

Effects of pH or ionic strength on nanosheets

To examine the pH sensitivity of RT nanosheets, the glass-bottom dish with a RT nanosheet was filled with 3 ml PBS and incubated at 37°C overnight. The solution was changed to 3 ml Britton–Robinson (B–R) buffer (40 mM H_3BO_3, 40 mM H_3PO_4, and 40 mM CH_3COOH, pH 7.0, adjusted by NaOH), and the dish was incubated on a sample stage for 15 min at 25°C. Then, the images were captured as in temperature sensitivity experiments. Next, after 1 ml of solution was removed, 1 ml B–R buffer (pH 10 adjusted by NaOH) was added, and the solution was pipetted five times. The final pH was 8 due to the linear pH-buffering capacity of B–R buffer. Then the images were captured under the same condition as that before changing the solution. The photobleaching effects were corrected by single-exponential fitting to the F.I. at pH 7.

To analyze the ionic strength sensitivity of RT nanosheets, the glass-bottom dish with a RT nanosheet was filled with 3 ml PBS and incubated at 37°C overnight. Then the solution was changed to 3 ml of 150 mM NaCl solution. The dish was incubated on a sample stage for 15 min to stabilize the temperature at 25°C. Images were captured as in temperature sensitivity experiments. After 1 ml of the solution was removed, 1 ml distilled water was added, and the solution was pipetted five times. The final concentration of NaCl was 100 mM. Images were captured under the same condition as that before changing the solution. To obtain the data at 0 mM NaCl, the initial solution was 3 ml distilled water. The photobleaching effects were corrected by single-exponential fitting to the F.I. at 150 mM.

Response speed of RT nanosheets

To analyze the response speed of RT nanosheets in response to a change in temperature, the glass-bottom dish with a RT nanosheet was filled with 3 ml PBS and incubated at room temperature (25°C) overnight. Then, the solution was replaced with 3 ml PBS. An inverted microscope (IX-73, Olympus) equipped with a Nipkow confocal scanner (CSU-X1, Yokogawa Electric) and an EMCCD camera (iXon Ultra, Andor Technology) were used for this measurement: viz., EuTTA was excited by a mercury lamp (Olympus) with an excitation filter (BP360–370, Olympus) and a dichroic mirror (FF409-Di03, Semrock). Rh101 was excited by a 561-nm laser light (Cobolt). A dichroic mirror (YOKO-T405/488/561, Semrock) and an emission filter (YOKO-FF01-617/73, Semrock) were used. The excitation and emission light were passed through the FF409-Di03 dichroic mirror in the microscope. The PlanApo N 60×/1.45 oil immersion objective lens (Olympus) was used. The local temperature was increased by the IR-LEGO system (Sigma Koki) with an infrared (IR) laser (λ = 1,475 nm, FPLD-1475-490-CP, FiberLabs). The duration of irradiation was controlled by a mechanical shutter, the signal of which was recorded with a data recorder (IX-408, iWorx). This experiment was performed at 24°C. Laser power through the objective lens at the specimen position was measured by a power meter (PowerMax-USB PM3, Coherent), and the area of 393 μm^2 at/around the laser spot was analyzed. In this experiment, the photobleaching effects were corrected by a quadratic function for the F.I. obtained before and after a laser irradiation, because the data were fitted more accurately than by an exponential function.

Temperature measurement for HeLa cells

HeLa cells were cultured on culture dishes (Techno Plastic Products) with Dulbecco's Modified Eagle's Medium (DMEM; Nacalai Tesque) containing 2 mM L-glutamine (Sigma-Aldrich), 10% FBS, 100 U/ml penicillin and 100 μg/ml streptomycin at 37°C with 5% CO_2. FBS, penicillin, and streptomycin were purchased from Thermo Fisher Scientific. A few days before experiments, cells were seeded on EuTTA or RT nanosheets.

HeLa cells on EuTTA or RT nanosheets were observed in 2 ml of HEPES-buffered saline solution (HBSS; 140 mM NaCl, 5 mM KCl, 1 mM $MgCl_2$, 1 mM Na_2HPO_4, 10 mM HEPES, 2 mM $CaCl_2$, and 5 mM D(+)-glucose, pH 7.4, adjusted by NaOH) at 36 ± 1°C. For chemical fixation, HeLa cells on RT nanosheets were incubated in PBS containing 4% paraformaldehyde (PFA; FUJIFILM Wako Pure Chemical) for 10 min at room temperature. For permeabilization, the fixed cells were incubated in PBS containing 1% (vol/vol) Triton X-100 (Nacalai Tesque). The fixed or permeabilized cells were also observed in 2 ml of HBSS. The microscopic system for the temperature sensitivity measurement (see above) was used for this experiment. 50 frames of fluorescence images of EuTTA or Rh101 were captured at an exposure time of 100 ms. 50 frames of background images were also captured with no excitation light, and thereby the average images from 50 frames were used to obtain normalized images.

In the experiments with trypsin, HeLa cells on EuTTA nanosheets were incubated in 2 ml culture medium containing 0.5 μM Calcein-AM (Dojindo Laboratories) for 30 min at 37°C

with 5% CO_2. After the solution was replaced with 2 ml HBSS, the cells were mounted on a sample stage. At 90 s after the onset of observation, 100 µl of 2.5% trypsin (Thermo Fisher Scientific) was added. The excitation filter was BP470–490 (Olympus) for the observation of Calcein. Non-stained HeLa cells on RT nanosheets were observed under the same conditions.

In the experiments with PFA, non-stained HeLa cells on EuTTA or RT nanosheets were observed in 2 ml HBSS. At 90 s after the onset of observation, 667 µl of 16% PFA (FUJIFILM Wako Pure Chemical) was added.

In the experiments with Triton X-100, HeLa cells on EuTTA nanosheets were incubated in 2 ml culture medium containing 0.5 µM Calcein-AM and 2.5 µg/ml CellMask Orange (Thermo Fisher Scientific) for 30 min at 37°C with 5% CO_2. Then, the cells were incubated in PBS containing 4% PFA for 10 min at room temperature. After changing the solution to 2 ml HBSS, the cells were mounted on a sample stage. At 90 s after the onset of observation, 200 µl of PBS containing 10% (vol/vol) Triton X-100 was added. The excitation filters for Calcein and CellMask Orange were BP470–490 (Olympus) and FF01-554/23 (Semrock), respectively. Non-stained HeLa cells on RT nanosheets were observed under the same conditions.

In the experiments with ionomycin, HeLa cells on RT nanosheets were incubated in HBSS containing 500 nM Fluo4-AM (Thermo Fisher Scientific) for 30 min at room temperature. The total DMSO concentration was 0.1%. After replacing the solution with 2 ml HBSS, the cells were mounted on a sample stage. At 90 s after the onset of observation, 20 µl of HBSS containing 200 µM ionomycin (10% DMSO; Sigma-Aldrich) was applied ~10 mm away from the observed cells. The excitation filter used for Fluo4 was FF01-469/35 (Semrock).

For temperature imaging of the ER, HeLa cells on EuTTA nanosheets were incubated in HBSS containing 500 nM Fluo4-AM and 50 nM ER thermo yellow for 30 min at room temperature. The total DMSO concentration was 0.1%. Subsequent experimental procedures were the same as those for RT nanosheets. The excitation filter for ER thermo yellow was FF01-554/23 (Semrock). The strength of excitation light for ER thermo yellow was adjusted to that used for Rh101 as in the experiments using RT nanosheets. In the experiments with thapsigargin, 40 µl of HBSS containing 100 µM ionomycin with or without 100 µM thapsigargin (Calbiochem, Merck; total 10% DMSO) was applied ~10 mm away from the observed cells.

The fluorescence images of stained cells and nanosheets (with or without cells) were analyzed by ImageJ software (National Institutes of Health [NIH]). The intensities were normalized by the average F.I. of 10 frames obtained at the onset of observation. The corrected F.I. of EuTTA or Rh101 was calculated as follows: viz., the normalized F.I. of EuTTA or Rh101 of nanosheets with cells was divided by that without cells. The corrected EuTTA/Rh101 F.I. ratio was simply obtained by the corrected EuTTA F.I. divided by the corrected Rh101 F.I.

Temperature measurement for cardiomyocytes

The primary cultured ventricular myocytes of neonatal Wistar rats (1 d) were obtained based on our previously published protocol (Shintani et al., 2014). RT nanosheets were hydrophilized with a magnetron spatter (MSP-10, Vacuum Device). The nanosheets were coated with 0.3 mg/ml collagen (Cellmatrix Type I-C, Nitta Gelatin) diluted in 1 mM HCl and incubated for 5 min at room temperature. Cardiomyocytes were cultured on collagen-coated RT nanosheets (5 mg/ml EuTTA, 12.5 µg/ml Rh101, and 10 mg/ml PMMA) in DMEM containing 4 mM L-glutamine (Sigma-Aldrich), 1 mM sodium pyruvate (FUJIFILM Wako Pure Chemical), 10% FBS, 100 U/ml penicillin, and 100 µg/ml streptomycin at 37°C with 5% CO_2.

At 4–5 d in vitro, cardiomyocytes on RT nanosheets were incubated in 1.8 mM Ca^{2+}-HEPES-Tyrode's solution (137 mM NaCl, 5.4 mM KCl, 0.5 mM $MgCl_2$, 0.33 mM NaH_2PO_4, 5 mM HEPES, and 5 mM D(+)-glucose, pH 7.4, adjusted by NaOH) containing 1 µM Fluo4-AM for 30 min at room temperature. After changing the solution to 2 ml of 1.8 mM Ca^{2+}-HEPES-Tyrode's solution, the cells were mounted on a sample stage and observed at 36°C under the same microscope as that used for HeLa and HEK293 cells. The frame rate was set at 33.3 Hz. Electrical stimulation (~20 V/cm, 1 ms, and 2 Hz) was applied by an electronic stimulator (SEN-3301, Nihon Kohden) and an isolator (SS-104J, Nihon Kohden; Tsukamoto et al., 2016). The electrical signal and shutter signal of the EMCCD camera were recorded by a data recorder (IX-404, iWorx).

The F.I. of Fluo4 in cardiomyocytes and that of RT nanosheets with cells were analyzed by ImageJ. The initial time of electrical stimuli was set at time 0. Fluo4 F.I. was normalized by the minimal F.I. obtained during observation. The F.I. of RT nanosheets with Fluo4-loaded or unloaded cells was measured. The F.I. of RT nanosheets was normalized by the averaged F.I. of 10 frames at the onset of observation. The photobleaching effects of RT nanosheets were corrected by a quadratic function fitted to the F.I. before and after the stimuli (see above). The F.I. of both Fluo4 and RT nanosheets was averaged. Likewise, the averaged F.I. of each stimulus was superimposed.

Temperature measurement for neurons

Hippocampal neurons were dissected from 17–19-d-old Wistar rat embryos based on our published protocol (Oyama et al., 2015). EuTTA nanosheets (5 mg/ml EuTTA and 10 mg/ml PMMA) on polymer-bottom dishes (Fine Plus International) were pretreated with collagen and poly-D-lysine based on our published protocol (Oyama et al., 2015): viz., the dishes were coated with 0.3 mg/ml collagen diluted in 1 mM HCl and incubated for 60 min at 37°C with 5% CO_2. After removing the collagen solution and drying for 5–30 min at room temperature, the dishes were washed twice with PBS and treated with 0.1 mg/ml poly-D-lysine (Millipore, Merck) diluted in sterilized distilled water for over 1 h at 37°C with 5% CO_2. The poly-D-lysine solution was removed and the dishes were dried for 5–30 min at room temperature, washed with sterilized distilled water three times, and filled with 1.6 ml of culture medium (Neurobasal medium containing 2% B-27 supplement, 81.4 µg/ml L-glutamine, 100 U/ml penicillin, and 100 µg/ml streptomycin, all purchased from Thermo Fisher Scientific). Then, the culture medium (400 µl) containing 4.0×10^5 cells was added to the dishes. The cells were cultured at 37°C with 5% CO_2 for 13–17 d before observation.

The neurons on an EuTTA nanosheet were incubated in HBSS (140 mM NaCl, 5 mM KCl, 1 mM $MgCl_2$, 1 mM Na_2HPO_4, 10 mM HEPES, 2 mM $CaCl_2$, and 10 mM D(+)-glucose, pH 7.4, adjusted by NaOH) containing 100 nM Fluo4-AM for 30 min at 37°C with 5% CO_2. After replacing the solution with 2 ml HBSS, the cells were mounted on a sample stage and observed at 36°C by an inverted microscope (IX-70, Olympus) with an EMCCD camera (iXon EM+ 897, Andor Technology). EuTTA and Fluo4 were excited using a SPECTRA Light Engine (377/50 nm, 485/20 nm; Lumencor) and observed with a PlanApo N 60×/1.45 oil immersion objective lens (Olympus). A dichroic mirror DM505 (Olympus) and an emission filter BA515IF (Olympus) were used. The temperature was adjusted by a thermostatically controlled incubator on the sample stage (INUG2-ONICS; Tokai Hit). Electrical stimulation (~5 V/cm, 10 ms, and 0.25 Hz) was applied by an electronic stimulator (SEN-7203, Nihon Kohden). The electrical signal and shutter signal of EMCCD camera were recorded by a data recorder (IX-408, iWorx). The frame rate was set at 38.5 Hz.

Changes in the F.I. of Fluo4 in somas or neurites in response to electrical stimuli were analyzed by ImageJ. The F.I. of EuTTA nanosheets with or without somas or neurites was measured. The F.I. of Fluo4 or EuTTA was normalized by the average F.I. of 50 frames before each stimulation. To correct fluctuations of excitation light and photobleaching of EuTTA, the normalized EuTTA F.I. for somas or neurites was divided by the F.I. obtained from the region where neither was present. The corrected F.I. was averaged and superimposed as in the analyses on cardiomyocytes.

Statistics

Data distribution for normality was assessed with the Kolmogorov–Smirnov test and the variance homogeneity with the Bartlett test. The Tukey–Kramer test was applied under parametric conditions and the Steel–Dwass test under nonparametric conditions. All of these statistical analyses were performed by R language and the Mann–Whitney *U* test by OriginPro2016 (OriginLab). ***, $P < 0.001$. n.s. indicates not significant ($P > 0.05$). Data are expressed as mean ± SEM unless otherwise noted. *n* indicates the number of experiments.

Online supplemental material

Fig. S1 shows the changes in the F.I. of EuTTA nanosheets with HeLa cells before and after treatment with trypsin, PFA, or Triton X-100. Fig. S2 shows the temperature sensitivity of EuTTA or Rh101 of a RT nanosheet. Fig. S3 shows the stability of RT nanosheets at various pH levels. Fig. S4 shows the stability of RT nanosheets at various ionic strengths. Fig. S5 shows the culture of HeLa cells on RT nanosheets. Fig. S6 gives the normalization procedure for fluorescence images of RT nanosheets. Fig. S7 shows changes in the F.I. of RT nanosheets with HeLa cells before and after treatment with trypsin, PFA, or Triton X-100. Fig. S8 shows the temperature measurement for HEK293 cells expressing malignant hyperthermia-causing RYR type 1 (RYR1) mutants. Fig. S9 shows the temperature measurement for HeLa cells on RT nanosheets upon ionomycin treatment. Fig. S10 shows the temperature measurement for the ER in HeLa cells on EuTTA nanosheets upon ionomycin treatment. Fig. S11 shows the temperature measurement for carbonyl cyanide m-chlorophenyl hydrazine (CCCP)–induced thermogenesis in rat neonatal cardiomyocytes. Fig. S12 shows the temperature measurement for CCCP-induced thermogenesis in brown adipocytes derived from WT-1 cells. Fig. S13 shows the temperature measurement for CCCP-induced thermogenesis in mouse brown adipocytes. Video 1 shows trypsin treatment for HeLa cells cultured on an EuTTA nanosheet. Video 2 shows skinning treatment for fixed HeLa cells cultured on an EuTTA nanosheet. Video 3 shows time-lapse images of HeLa cells cultured on a RT nanosheet. Video 4 shows ionomycin treatment for HeLa cells cultured on a RT nanosheet. Video 5 shows ionomycin treatment of HeLa cells stained with ER thermo yellow cultured on an EuTTA nanosheet. Video 6 shows Ca^{2+} imaging of beating cardiomyocytes cultured on a RT nanosheet. Video 7 shows bright-field images of beating cardiomyocytes cultured on a RT nanosheet. Video 8 shows Ca^{2+} imaging of exciting neurons cultured on an EuTTA nanosheet.

Results

The fluorescent thermometer nanosheets composed of EuTTA and PMMA are reportedly useful for temperature mapping (see Kolodner and Tyson 1982; Itoh et al., 2014), with the F.I. of the nanosheet decreasing in response to an increase in temperature. In the present study, we cultured various types of cells on the nanosheet to measure the difference in temperature between living cells and the medium. Should living cells be warmer than the medium, the following results would be yielded: (a) The F.I. of the nanosheet under living cells is lower than that in the medium, (b) the F.I. increases and becomes similar to that in the medium once living cells are detached from the nanosheet, and (c) unlike living cells, dead cells do not decrease the F.I.

First, we performed temperature mapping for cultured HeLa cells on the nanosheet. We found that the F.I. was lower for HeLa cells than the medium: viz., when the cells were detached from the nanosheet upon trypsin treatment, the F.I. became similar to that for the medium (Fig. S1, A–D; and Video 1). This demonstrates that the nanosheet was well maintained during cell culture. These findings are in line with the notion that temperature is higher in living cells than the medium. However, the F.I. for the chemically fixed (PFA-treated) cells (i.e., dead cells) was likewise lower than the medium (Fig. S1, E–G). Although permeabilization of the fixed cells with Triton X-100 (0.9% [vol/vol]) increased the F.I. by a small magnitude (~4%), it was still lower than the medium (Fig. S1, H–L; and Video 2). It is therefore likely that the F.I. of the nanosheet for cells is sensitive to nonthermal factors as well. Because the presently obtained fluorescence images were similar to those captured by an interference reflection microscopy (compare with Curtis, 1964; Verschueren, 1985), the following scenario may account for the above findings: viz., the EuTTA fluorescence interferes with the reflected fluorescence by the cellular membrane and intracellular components. Accordingly, the EuTTA fluorescence becomes lower in regions where cells are located, regardless of the cellular temperature.

Then, in order to correct for the interference effect, we developed RT nanosheets composed of EuTTA and the temperature-insensitive fluorescent dye Rh101 (Fig. 1, A and B), based on our previously reported nanoparticles (Takei et al., 2014). The emission peaks were 612 and 587 nm for EuTTA and Rh101, respectively (Takei et al., 2014), suggesting that the interference effect of EuTTA is similar to that of Rh101. We therefore assumed that the ratio of their F.I. values, rather than the absolute values, should be used for the correction of temperature measurement with nanosheets. The thickness and surface roughness of RT nanosheets were 52.3 ± 4.7 nm and 0.36 ± 0.04 nm, respectively (mean ± SD; n = 3 nanosheets with three measurements performed for each nanosheet). While the F.I. of EuTTA decreased linearly with increasing temperature from 25 to 40°C (−3.42%/°C at 36°C; Fig. 1 C and Fig. S2), that of Rh101 was unaffected by the temperature change (−0.06%/°C; Fig. 1 C). It is therefore likely that the EuTTA/Rh101 ratio provides a linear relationship for a change in temperature (−3.35%/°C at 36°C; Fig. 1 D). When pH was varied in the range of 5–9, the F.I. of both EuTTA and Rh101 and the EuTTA/Rh101 ratio remained stable within ±0.5% (Fig. 1, E and F; and Fig. S3). When ionic strength was varied by NaCl in the range of 0–450 mM, the F.I. remained likewise constant within ±1.5% (Fig. 1, G and H; and Fig. S4). We then tested whether or not RT nanosheets respond to a rapid change in temperature. By taking advantage of an IR laser beam (λ = 1,475 nm; see Oyama et al., 2015; Ishii et al., 2019), we instantaneously increased temperature in the solution on the RT nanosheet from 24°C to 28°C around the laser spot (Fig. 1, I and J). The F.I. of EuTTA decreased within one frame (10.5 ms) upon onset of laser irradiation and returned to the preirradiation level after cessation of irradiation, again, within one frame (Fig. 1, J and K). These findings led us to conclude that our newly developed RT nanosheets can be used for temperature measurement at a speed of at least ∼100 Hz (note that the speed is limited by the capture speed, but not by the optical property of RT nanosheets). In contrast, the F.I. of Rh101 was hardly changed during IR laser irradiation (Fig. 1, J and K).

By taking advantage of the above characteristics of RT nanosheets, we investigated whether or not living cells are warmer than the medium, first by proliferating HeLa cells on the nanosheets (Fig. S5 A; and Video 3). A live/dead assay did not detect a significant difference in viability between glass-bottom culture dishes (live cells, 93.6 ± 1.3%) and RT nanosheets (live cells, 92.3 ± 1.0%), 3 d after seeding (Fig. S5, B and C). We measured the F.I. of RT nanosheets for HeLa cells: the normalized F.I. of the nanosheet with cells was lower by 6.1 ± 0.2% and 6.0 ± 0.4% for EuTTA and Rh101, respectively, than for the medium (i.e., without cells; Fig. 2, A and B; and Fig. S6). Following trypsin treatment, the EuTTA/Rh101 ratio became similar to that for the medium (Fig. S7, A and B). After fixation with PFA, the normalized F.I. remained low for both EuTTA (−6.0 ± 0.2%) and Rh101 (−6.1 ± 0.3%; Fig. 2, A and B; and Fig. S7, C and D). Although the treatment with Triton X-100 increased both F.I. values by a small magnitude, they remained lower than that for the medium (i.e., EuTTA, −3.1 ± 0.1%; Rh101, −3.3 ± 0.3%; Fig. 2, A and B; and Fig. S7, E and F). These findings are consistent with the notion that both EuTTA and Rh101 F.I. are influenced by nonthermal factors. Thus, the ratio maps of the fluorescence images were obtained to exclude the nonthermal factors; viz., the intensity ratio (i.e., EuTTA/Rh101) in living cells became 1.0014 ± 0.0027, which was similar to the value in the medium (Fig. 2, A and B; and Fig. S6). Likewise, the intensity ratios for fixed and skinned cells were 1.0024 ± 0.0021 and 1.0038 ± 0.0032, respectively (Fig. 2, A and B). The 95% confidence interval (1.96 × SEM) was 0.41–0.63% (i.e., 0.12–0.19°C). These data show that the global cellular temperature of living cells is similar to that of permeabilized or chemically fixed cells on RT nanosheets, or that in the medium, within ∼0.2°C.

Next, we performed temperature mapping for HEK293 cells expressing RYR1 with mutations (R164C or Y523S) that reportedly cause malignant hyperthermia (Fig. S8 A; cf. Murayama et al., 2015). Murayama et al. (2015) reported that either type of the mutated RYR1 promotes a leak of Ca^{2+} from intracellular Ca^{2+} stores, i.e., ER, resulting likely in enhancement of endogenous heat production via activation of SR/ER Ca^{2+}-ATPase (SERCA) proteins. In the present study, HEK293 cells expressing either RYR1 (WT), RYR1 (R164C), or RYR1 (Y523S) were cultured on RT nanosheets (Fig. S8 B). Consistent with the data on HeLa cells (Fig. 2), both EuTTA and Rh101 F.I. were lower for HEK293 cells than the medium (Fig. S8, C and D). Significant differences in the EuTTA/Rh101 ratio were not observed between the groups (i.e., control [with no induction of RYR1 expression], 1.0022 ± 0.0020; HEK293+RYR1 [WT], 1.0030 ± 0.0012; HEK293+RYR1 [R164C], 1.0023 ± 0.0017; HEK293+RYR1 [Y523S], 1.0028 ± 0.0021; Fig. S8 D). The 95% confidence interval was 0.24–0.41% (i.e., 0.07–0.12°C). These data therefore demonstrate that despite the heat presumably produced in the micrometer domains at/around SERCA proteins, due to a leak of Ca^{2+} from RYR1 (hence higher baseline cytosolic calcium concentration, $[Ca^{2+}]_{cyt}$) in cells expressing RYR1 (R164C) or RYR1 (Y523S), the temperature was not increased by greater than ∼0.1°C at the whole cell level.

Earlier we reported that the treatment with ionomycin, a Ca^{2+} ionophore, increases the temperature in HeLa cells (Suzuki et al., 2007; Takei et al., 2014; Arai et al., 2014; Itoh et al., 2016), as well as in NIH/3T3 cells (Yang et al., 2011), accompanied by a marked increase in $[Ca^{2+}]_{cyt}$. We therefore tested in the present study whether or not RT nanosheets yield detection of the ionomycin-induced temperature increase of HeLa cells. When ionomycin (2 μM) was applied to HeLa cells on RT nanosheets, $[Ca^{2+}]_{cyt}$ was markedly increased, as indicated by an increase in Fluo4 F.I. (Fig. 3, A and B; Fig. S9 A; and Video 4). Ionomycin increased EuTTA F.I. for both HeLa cells and the medium (Fig. S9 B), with a greater increase for HeLa cells than the medium (Fig. S9 B). A similar result was obtained with Rh101 (Fig. S9 C), and the EuTTA/Rh101 ratio was increased to a level similar as that for the medium (Fig. S9 D).

Next, in order to eliminate the cell-independent influence on the F.I. of RT nanosheets, the F.I. for cells was divided by that for the medium (Fig. 3 C and Fig. S9, E–G). The corrected F.I. for both EuTTA and Rh101 showed similar responses to ionomycin application (Fig. S9, E and F), and the ratio was steady with time, i.e., within an error of ±0.05% (± ∼0.15°C). The treatment with DMSO (0.1%; i.e., solvent for ionomycin) did not affect $[Ca^{2+}]_{cyt}$;

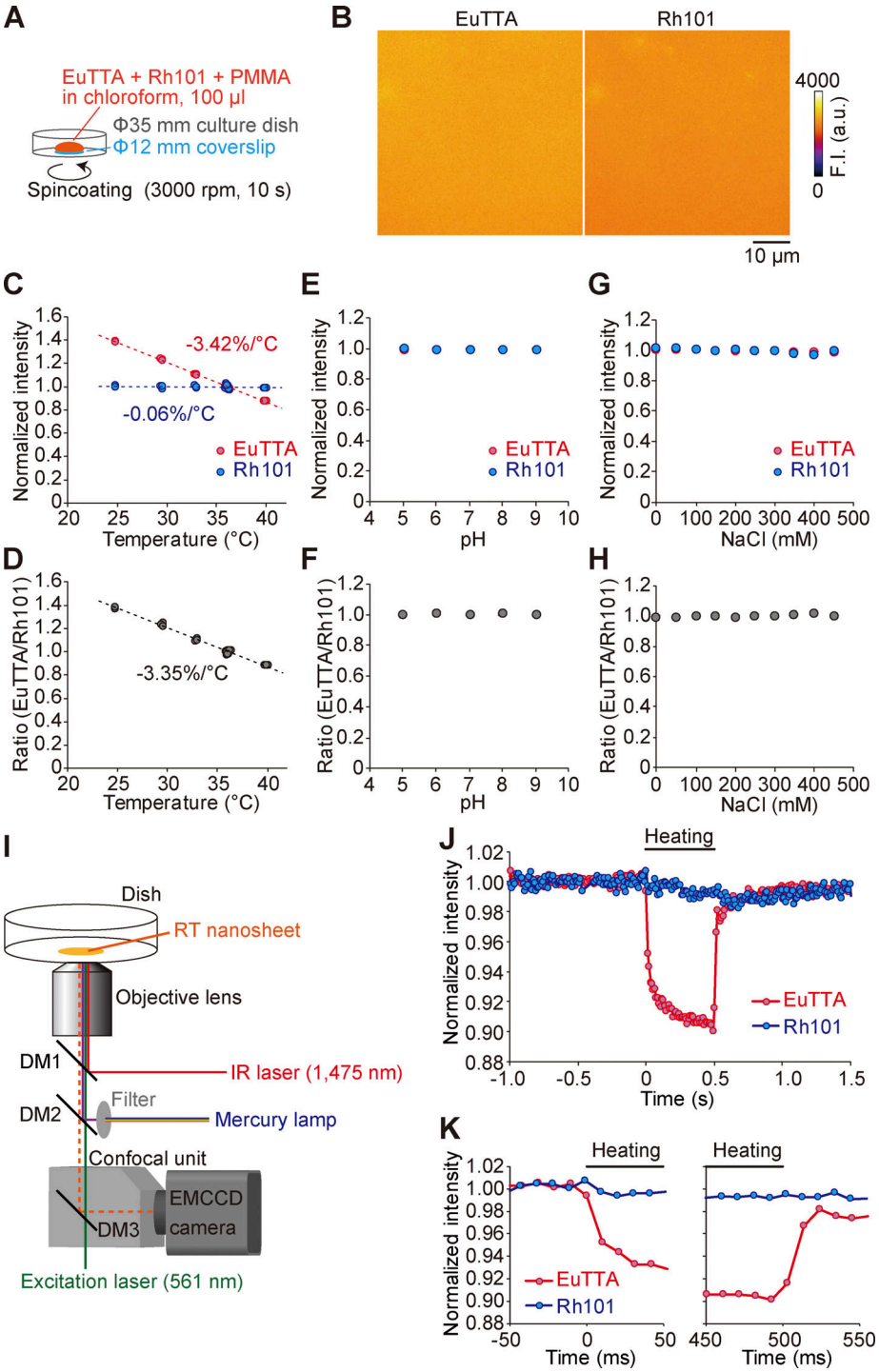

Figure 1. **Fluorescence characteristics of RT nanosheets. (A)** Illustration showing preparation of a RT nanosheet; viz., chloroform (volume of 100 µl), containing the temperature-sensitive fluorescent dye EuTTA, the temperature insensitive fluorescent dye Rh101 and PMMA, is spin-coated on a coverslip of a culture dish. **(B)** Fluorescence images of EuTTA (left) and Rh101 (right) of a RT nanosheet. F.I. is expressed in arbitrary units (a.u.). **(C)** Temperature dependence of the F.I. of EuTTA (red) and Rh101 (blue). F.I. normalized at 36°C for both EuTTA and Rh101. Slopes, −3.42 and −0.06%/°C for EuTTA and Rh101, respectively. n = 3. See Fig. S2. **(D)** Temperature-dependence of the EuTTA/Rh101 ratio. Slope, −3.35%/°C. **(E)** F.I. of EuTTA (red) and Rh101 (blue) at various pH levels. Note that red circles overlap with blue circles. F.I. normalized at pH 7. n = 3. **(F)** EuTTA/Rh101 ratio at various pH levels. **(G)** F.I. of EuTTA (red) and Rh101 (blue) at various ionic strengths. F.I. normalized at 150 mM. n = 3. See Fig. S4. **(H)** EuTTA/Rh101 ratio at various ionic strengths. In E–H, error bars (SEM) are within plots. **(I)** Illustration showing a microscopic system for optical heating of a RT nanosheet. Focused IR laser (λ = 1,475 nm; 8 mW) increased temperature around the laser spot. DM, dichroic mirror; DM1, custom-made DM (Sigma Koki); DM2, FF409-Di03 (Semrock); DM3, YOKO-T405/488/561 (Semrock). The optical paths are simplified. See Materials and methods for details. **(J)** Time-course of changes in the F.I. of an RT nanosheet upon an increase in temperature by IR laser irradiation for 0.5 s (as indicated by "Heating"). F.I. around the laser spot (393 µm^2) was measured. F.I. was normalized by that obtained before heating. The photobleaching effects were corrected. **(K)** Enlarged graphs of J showing the onset (left) and end (right) of heating.

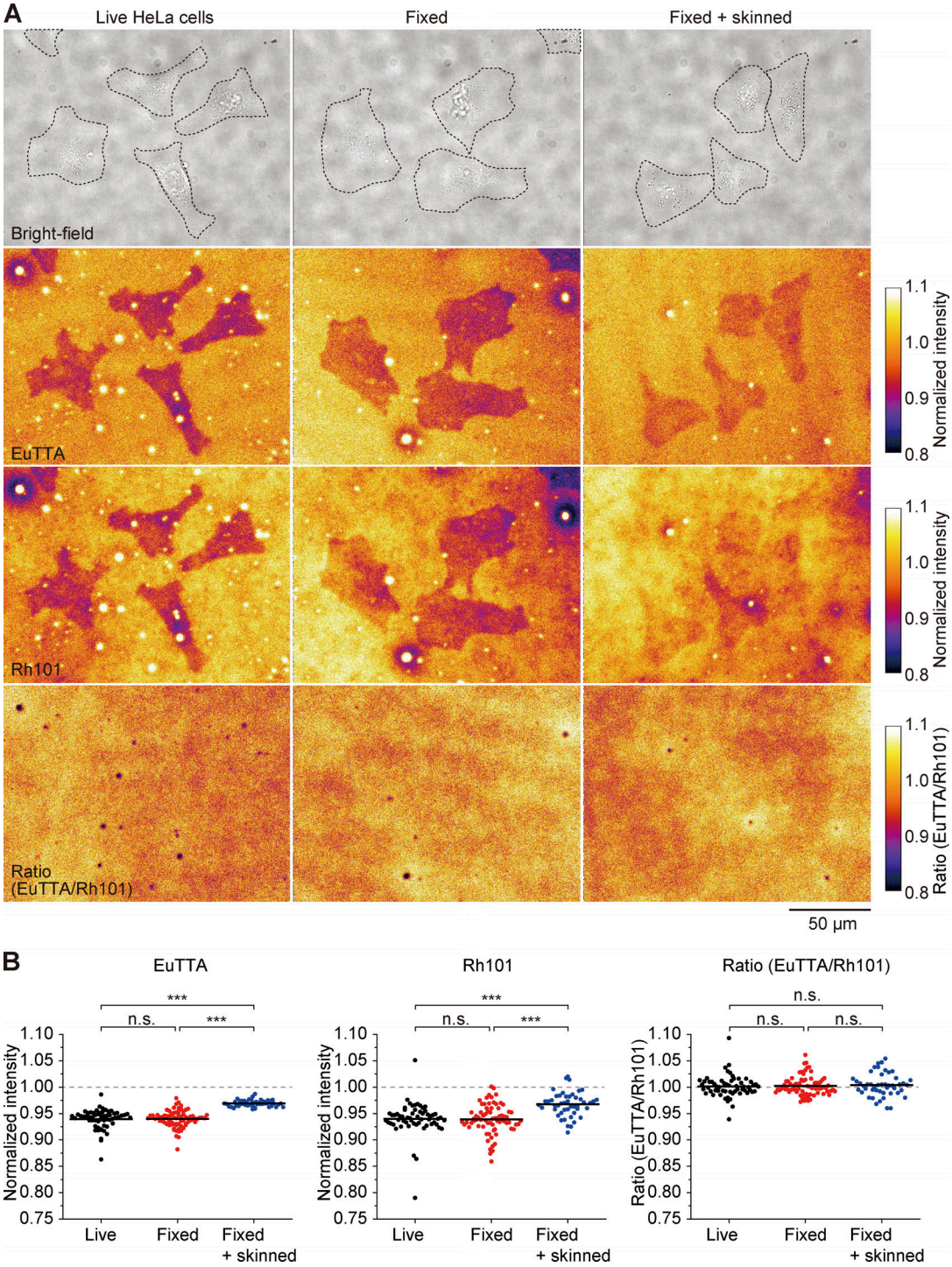

Figure 2. **Temperature-mapping of HeLa cells on RT nanosheets. (A)** From top to bottom: Bright-field image, fluorescence image of EuTTA, fluorescence image of Rh101, and the EuTTA/Rh101 ratio image on a RT nanosheet. HeLa cells were cultured on a RT nanosheet. Left, center, and right columns indicate live cells, fixed cells, and skinned cells after fixation, respectively. Dashed lines in bright-field images indicate the outlines of cells. F.I. was normalized by that of the RT nanosheet without cells. See Fig. S5. **(B)** Comparison of normalized F.I. for EuTTA (left) and Rh101 (middle), and the EuTTA/Rh101 ratio (right) between live cells, fixed cells, and skinned cells after fixation. Number of cells, 58, 73, and 47 for live cells, fixed cells, and skinned cells after fixation, respectively. For EuTTA and Rh101, the Steel–Dwass test was performed. For the EuTTA/Rh101 ratio, the Tukey–Kramer test was performed. ***, $P < 0.001$; n.s., not significant.

however, it increased EuTTA F.I. with either HeLa cells or the medium (~2.5%; Fig. 3, B and C; and Fig. S9, H–N). Therefore, EuTTA F.I. was sensitive to the DMSO treatment, although the F.I. was unaffected by a change in pH or ionic strength (Fig. 1, E–H). During DMSO treatment, corrected intensities were stable for both EuTTA and Rh101 compared with ionomycin treatment (Fig. S9), presumably because the ionomycin-induced cellular deformation or detachment from the nanosheet (Video 4) is

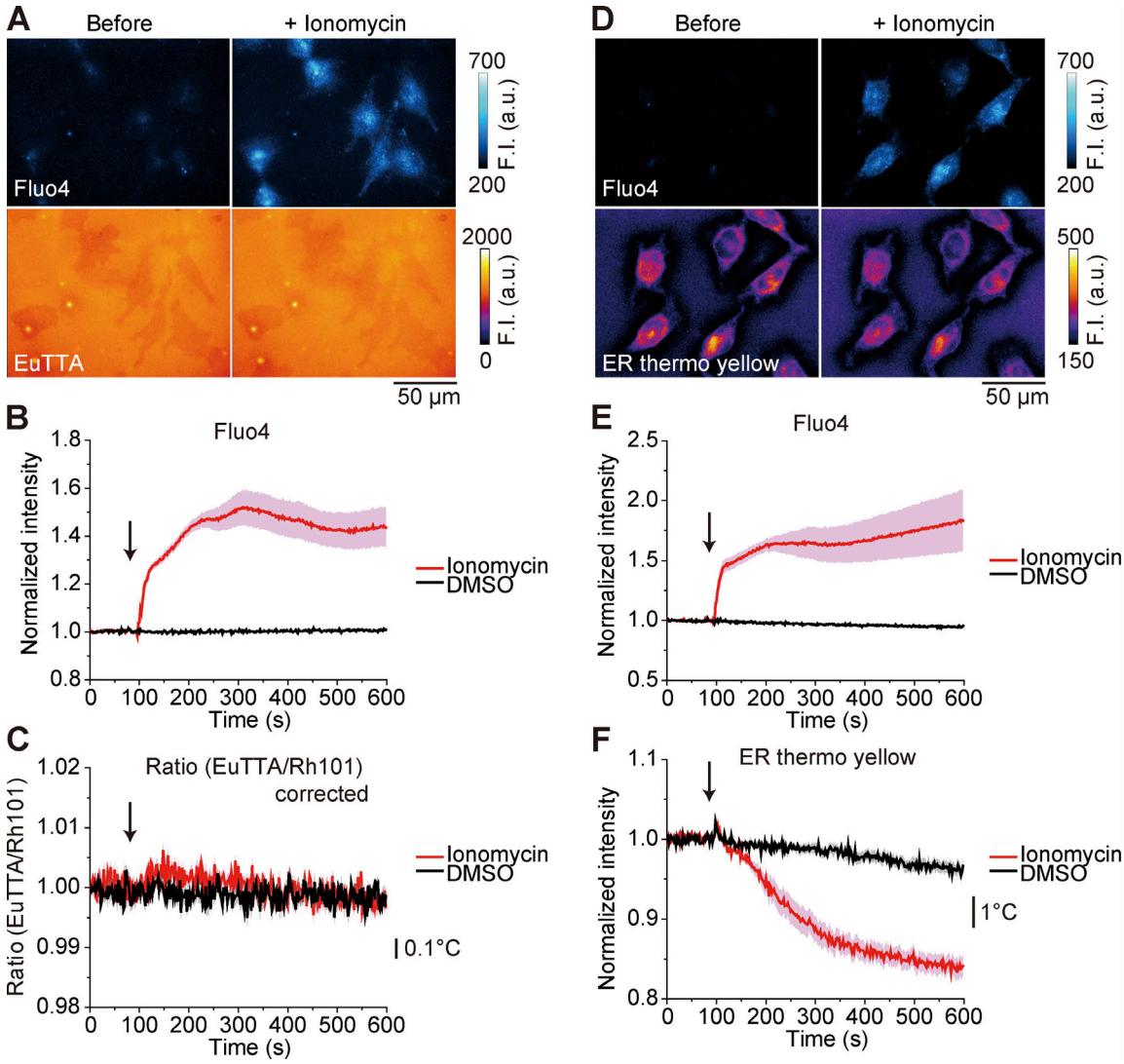

Figure 3. **Temperature measurement for HeLa cells. (A)** Fluorescence images of Fluo4 (top) in HeLa cells and EuTTA (bottom) of a RT nanosheet. Left and right: Before and after induction of Ca^{2+} increases by 2 μM ionomycin, respectively. See Video 4. **(B)** Time course of changes in the F.I. of Fluo4 in HeLa cells on RT nanosheets before and after application of ionomycin (red line) or DMSO (black line). **(C)** Time course of the EuTTA/Rh101 ratio of RT nanosheets with cells. F.I. corrected by that for the medium. See Fig. S9. In B and C: number of cells, 16 (n = 3) and 10 (n = 2) for ionomycin and DMSO, respectively. Data shown as mean ± SEM. The arrow indicates the point at which ionomycin or DMSO was applied. **(D)** Fluorescence images of Fluo4 (top) and ER thermo yellow (bottom) in HeLa cells on an EuTTA nanosheet. Left and right: Before and after induction of Ca^{2+} increases by 2 μM ionomycin, respectively. See Video 5. **(E)** Time course of changes in Fluo4 F.I. in HeLa cells on EuTTA nanosheets before and after application of ionomycin (red line) or DMSO (black line). **(F)** Time course of changes in the F.I. of ER thermo yellow in HeLa cells on EuTTA nanosheets. In E and F: number of cells, 12 (n = 3) and 8 (n = 2) for ionomycin and DMSO, respectively. Data shown as mean ± SEM. The arrow indicates the point at which ionomycin or DMSO was applied. Calibration bars in C and F were calculated from the temperature sensitivity of RT nanosheets (−3.35%/°C, cf. Fig. 1 D) and ER thermo yellow (−3.9%/°C; cf. Arai et al., 2014), respectively. Fluorescence images in A and D are averaged from 30 frames before (0–58 s) and after (180–238 s) the ionomycin treatment. a.u., arbitrary units.

likely to increase the F.I. of nanosheets, as observed during trypsin treatment (Fig. S7, A and B).

To confirm the ionomycin-induced increase in intracellular temperature, therefore, the ER-targeted fluorescent thermometer ER thermo yellow (see Arai et al., 2014) was loaded into HeLa cells on EuTTA nanosheets. ER thermo yellow is a small molecule fluorescent thermometer with high temperature sensitivity (−3.9%/°C), which reportedly stains the ER/SR in various types of cells, such as HeLa cells, brown adipocytes, and C2C12 myotubes (Arai et al., 2014, Itoh et al., 2016). During ionomycin treatment, ER thermo yellow F.I. decreased, as compared with DMSO treatment (Fig. 3, D–F; Fig. S10, A–D; and Video 5). The F.I. during ionomycin treatment was ~10% lower than during DMSO treatment, indicating that the local temperature at the ER increases by greater than ~2°C (Fig. 3 F), and the magnitude of rise in temperature was comparable to the results of our previous studies performed under different experimental settings (Arai et al., 2014; Itoh et al., 2016). Consistent with this notion, the magnitude of decrease in ER thermo yellow F.I. became less pronounced in the presence of thapsigargin (2 μM), an inhibitor of SERCA proteins (as in Suzuki et al., 2007). Therefore, it can be said that ionomycin treatment increases the local temperature at

the ER by ∼2°C or higher; however, when measured from the outside of the cell, the global cellular temperature remains nearly constant within ±0.2°C.

Intracellular thermometries have reportedly enabled detection of mitochondrial temperature in various types of cells, especially when stimulated by an uncoupling reagent such as carbonyl cyanide-p-trifluoromethoxyphenylhydrazone (FCCP) or CCCP (Gota et al., 2009, Okabe et al., 2012, Kiyonaka et al., 2013, Tanimoto et al., 2016, Nakano et al., 2017, Kriszt et al., 2017). To the best of our knowledge, Gota et al. (2009) were the first to report an increase in temperature by ∼0.45°C in COS7 cells upon application of 100 μM FCCP. Okabe et al. (2012) reported that the temperature is higher near mitochondria in COS7 cells upon application of 100 μM FCCP. Kiyonaka et al. (2013) expressed the fluorescent thermometer protein tsGFP1-mito in the mitochondrial intima of HeLa cells or brown adipocytes, and observed an increase in temperature upon application of 10 μM CCCP in both types of cells. Kriszt et al. (2017) applied the ER-targeted thermometer ERthermAC to brown adipocytes (derived from WT-1 brown preadipocytes) and observed an increase in temperature at the ER upon application of 10 μM FCCP. Based on these previous reports, we performed global thermometry with RT nanosheets combined with intracellular thermometry for the ER/SR with ER thermo yellow in cardiomyocytes and adipocytes to compare global versus local temperature when mitochondria were uncoupled by CCCP. As pointed out by Kriszt et al. (2017), (a) temperature measurement in mitochondria can potentially be affected by a change in the physical or chemical properties of mitochondria, such as membrane potential (Arai et al., 2015), and (b) mitochondria-associated ER membranes provide sufficiently close proximity of these two organelles, we measured the local temperature at the ER/SR as an index of "mitochondrial temperature" (Supplemental text, see bottom of PDF).

First, we performed extracellular and intracellular temperature measurements on cardiomyocytes because they are widely regarded as mitochondria-rich cells (Else and Hulbert, 1985). When 10 μM CCCP was applied to neonatal cardiomyocytes on RT nanosheets, the EuTTA/Rh101 ratio remained nearly stable within ±0.3% (≈ ±0.1°C), and the result was similar to that obtained by using the solvent (0.1% DMSO; Fig. S11, A and B). We then costained cardiomyocytes with ER thermo yellow and ER tracker green, because ER tracker green is reportedly insensitive to a change in temperature (Arai et al., 2014). When cardiomyocytes were heated via IR-laser irradiation, the F.I. of ER thermo yellow was consistently decreased while that of ER tracker green remained nearly stable (Fig. S11, C and D). With the application of 10 μM CCCP, the F.I. of ER thermo yellow decreased (Fig. S11 E). The speed of onset of the decrease in the F.I. was slightly faster with 10 μM CCCP than 0.1% DMSO, suggesting that temperature may be increased at the SR via thermogenesis of mitochondria uncoupling. However, the F.I. of temperature-insensitive ER tracker green likewise decreased upon application of 10 μM CCCP, with a magnitude much larger than that obtained by temperature-sensitive thermo yellow (Fig. S11 F). Moreover, 10 μM rotenone (i.e., an inhibitor of mitochondrial respiratory chain complex I) did not suppress the decrease in the F.I. of either ER thermo yellow or ER tracker green (Fig. S11, G and H). It is therefore likely that the observed F.I. decrease of either ER thermo yellow or ER tracker green is due to a CCCP-induced change in intracellular nonthermal factors.

Next, we performed the same experiments on brown adipocytes. We cultured WT-1 brown preadipocytes on RT nanosheets and differentiated them to adipocytes (Fig. S12 A). When 10 μM CCCP was applied to brown adipocytes on RT nanosheets, the EuTTA/Rh101 ratio remained nearly stable within ±0.3% (≈ ±0.1°C), and the result was similar to that obtained by using the solvent (0.1% DMSO; Fig. S12, A and B). The F.I. of ER thermo yellow decreased while that of ER tracker green hardly changed upon an increase in temperature via IR-laser irradiation (Fig. S12, C and D). When 10 μM CCCP was applied, the F.I. of ER thermo yellow and that of ER tracker green decreased by a similar magnitude (Fig. S12, E and F), which was not suppressed by preincubation with 10 μM rotenone (Fig. S12, G and H). Similar results were yielded on the brown adipocytes derived from mouse brown preadipocytes: viz., when 10 μM CCCP was applied, (a) the EuTTA/Rh101 ratio remained nearly stable within ±0.5% (≈ ±0.15°C; Fig. S13, A and B), and (b) the F.I. of not only ER thermo yellow but also ER tracker green decreased (Fig. S13, C–E). Therefore, the present findings on cardiomyocytes and brown adipocytes suggest that mitochondria uncoupling does not change global cellular temperature by a detectable magnitude (i.e., ± ∼0.1°C).

In excitable cells, such as cardiomyocytes and neurons, $[Ca^{2+}]_{cyt}$ changes in a repeated fashion under physiological conditions. We therefore investigated whether or not RT nanosheets can detect changes in temperature in response to a change in $[Ca^{2+}]_{cyt}$ in cardiomyocytes, and then in neurons. Rat neonatal cardiomyocytes cultured on RT nanosheets exhibited spontaneous Ca^{2+} transients and contractions (Fig. 4, A and B; Video 6; and Video 7), and electrical stimuli at 2 Hz induced periodic $[Ca^{2+}]_{cyt}$ changes and subsequent contractions (Fig. 4 B, Video 6, and Video 7). During electric stimuli, the F.I. of RT nanosheets did not change by a detectable magnitude for individual myocytes (i.e., myocytes #1–#5; Fig. 4, A and B). Averaging the data of all cells (142 cells) revealed that the F.I. of both EuTTA and Rh101 repeatedly varied at 2 Hz (amplitude, ∼0.1%) in a reciprocal manner with Fluo4 F.I. (Fig. 4 C). To reduce the noise and, thereby, enhance the precision in temperature measurement, we superimposed the various F.I. signals obtained during the course of Ca^{2+} transients (total, 10; see Materials and methods for details; Fig. 4 D). It was accordingly found that the F.I. of both EuTTA and Rh101 decreased by ∼0.1%. Given the result that the EuTTA/Rh101 ratio remained stable within ±0.03% (Fig. 4 D), it is reasonable to conclude that the magnitude of change in temperature in physiologically beating cardiomyocytes is within ±0.01°C.

Rat hippocampal neurons that had been cultured on the EuTTA nanosheet exhibited spontaneous and electrically stimulated Ca^{2+} transients (Fig. 5, A and B; and Video 8). Temperature measurement on neurons was performed as follows: (a) the electrical stimuli-induced Ca^{2+} transients were confirmed, (b) the F.I. of EuTTA nanosheets was measured during stimulus

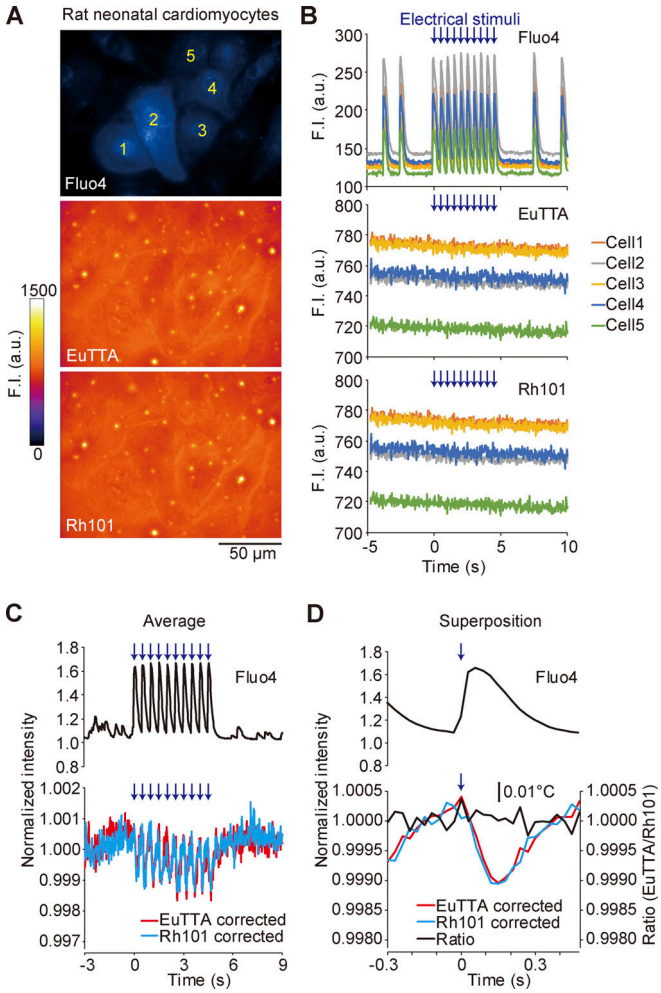

Figure 4. **Temperature measurement for rat neonatal cardiomyocytes. (A)** Fluorescence images of Fluo4 (top), EuTTA (middle), and Rh101 (bottom) of cardiomyocytes on a RT nanosheet. Images were averaged from 600 frames (for 18 s) during observation. **(B)** Time course of changes in the F.I. of Fluo4 (top), EuTTA (middle), and Rh101 (bottom). Data obtained from cells 1–5 (see A, top; Video 6, and Video 7). **(C)** Top: Time course of changes in average Fluo4 F.I. in cardiomyocytes on RT nanosheets. Number of cells, 75 (n = 17). Bottom: Time course of changes in the F.I. of EuTTA (red) and Rh101 (blue) on RT nanosheets cultured with cardiomyocytes. Different cells were used in top and bottom, and Fluo4 was not loaded in cells in bottom. The photobleaching effects were corrected. Number of cells, 142 (n = 36). See Materials and methods for details. **(D)** Superimposed data of Fluo4 (top), and EuTTA (red), Rh101 (blue), and EuTTA/Rh101 (black; bottom). Data obtained by 10 stimuli were superimposed. A calibration bar of 0.01°C was calculated from the temperature sensitivity of the EuTTA/Rh101 ratio (i.e., −3.35%/°C; cf. Fig. 1 D). Arrows in B, C, and D indicate the points at which electrical stimuli were applied. a.u., arbitrary units.

application, and (c) after temperature measurement, the Ca^{2+} transients were reconfirmed. Accordingly, we observed no detectable changes in EuTTA F.I. for either soma or neurites under activating conditions (Fig. 5 B). Fig. 5 C shows time-courses of changes in the average F.I. of Fluo4 (top) and EuTTA (bottom) for 53 somas (blue) and 48 neurites (red). As a result, despite clear Fluo4 F.I. signals occurring at each stimulation, EuTTA F.I. remained stable within ±0.1%. Superposition of data obtained by five stimulations further confirmed that the temperature

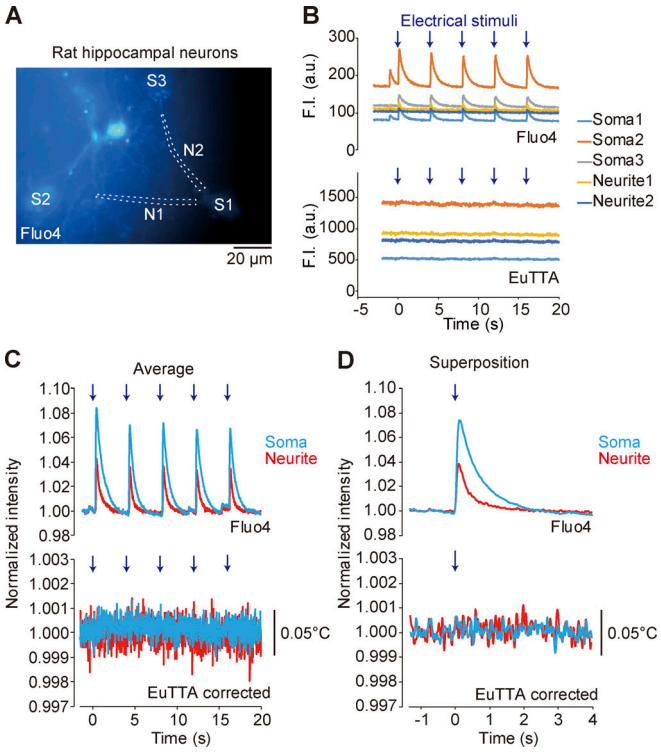

Figure 5. **Temperature measurement for rat hippocampal neurons. (A)** Fluorescence image of Fluo4 in neurons on an EuTTA nanosheet. Three somas (S1, S2, and S3) and two neurites (N1 and N2) were analyzed. Image averaged from 900 frames (for 23.4 s) during observation. **(B)** Time course of changes in the F.I. of Fluo4 (top) and EuTTA (bottom). See Video 8. **(C)** Top: Time course of changes in average Fluo4 F.I. in somas and neurites on EuTTA nanosheets. Bottom: Time course of changes in average EuTTA F.I. for somas and neurites. Number of somas and neurites, 53 and 48, respectively (n = 38). The same neurons were used in top and bottom. **(D)** Superimposed data of Fluo4 (top) and EuTTA (bottom). Data of 20 stimuli were superimposed. A calibration bar of 0.05°C was calculated from the temperature sensitivity of EuTTA nanosheets (i.e., −3.42%/°C; cf. Fig. 1 C). Arrows in B, C, and D indicate the points at which electrical stimuli were applied. a.u., arbitrary units.

remains stable within ±0.03°C for both soma and neurite upon stimulation (Fig. 5 D).

Discussion

The present experiments revealed that the 1°C order difference between cells and the medium was not detected at the whole cell level upon activation of SERCA proteins in either nonexcitable (HeLa/HEK293 cells) or excitable (cardiomyocytes and neurons) cells. These experimental findings are in line with previous theoretical calculations by us (Takei et al., 2014) and others (Yang et al., 2011, Baffou et al., 2014); viz., the metabolic heat production in a living cell (~100 pW) contributes to an increase in cellular temperature by only ~10µ°C. This is most typically reflected by the result that nonphysiological stimulation upon application of ionomycin increased intracellular temperature in the ER by greater than ~2°C; however, the magnitude of change in temperature at the cellular surface measured by RT nanosheets was within ±0.2°C (Fig. 3). It is therefore likely that SERCA proteins produce heat only locally during the ATPase

cycle, but not to the magnitude where cellular temperature is raised on a global cellular basis. This view is consistent with our earlier finding in that temperature was increased by ~1.6°C in the SR in C2C12 myotubes, while the cytoplasmic thermometry did not reveal a significant rise in temperature by a magnitude of greater than ~0.1°C (Itoh et al., 2016). It is therefore suggested that upon activation of SERCA proteins, both nonexcitable and excitable cells locally produce a small amount of heat, to efficiently use the thermodynamic energy to regulate various enzymatic reactions (such as SERCA proteins per se) and the open-close kinetics of ion channels, located just proximal to the heat source proteins (Tseeb et al., 2009; Itoh et al., 2014).

As described in the Introduction, intracellular thermometry is still challenging because it is difficult to exclude all of the nonthermal effects on thermometers. In the present study, we used ER thermo yellow for temperature measurement of ER in HeLa cells. Arai et al. (2014) reported that pH changes within a physiological range (5–8) had no effect on the temperature sensitivity of ER thermo yellow, and Ca^{2+} changes (0–0.8 mM) did not affect ER thermo yellow F.I. However, they also reported that the temperature sensitivity in live and fixed HeLa cells (−3.9%/°C) was different from that in HEPES buffer solution (−1.7%/°C), and suggested that the binding of ER thermo yellow to unknown biomolecules altered the sensitivity (Arai et al., 2014). Thus, ER thermo yellow is not a "perfect thermometer," because it is affected by nonthermal factors in cells. Therefore, a multidimensional explanation is necessary for the ionomycin-induced temperature changes detected by ER thermo yellow. The F.I. changes of ER thermo yellow detected a temperature increase at ER in HeLa cells induced by ionomycin (Arai et al., 2014), and a similar temperature increase was also detected by fluorescence lifetime imaging of ER thermo yellow, which was independent of ionic strength (0–500 mM KCl; Itoh et al., 2016). The spectral shift of quantum dots detected the ionomycin-induced thermogenesis in NIH/3T3 cells (Yang et al., 2011). Heterogeneous temperature increases in HeLa cells were detected by ratiometric thermometry with EuTTA/Rh101 nanoparticles, which were independent of pH (4–10), ionic strength (0–500 mM KCl), protein concentration (0–45 wt %), and viscosity (1–220 cP; Takei et al., 2014). Based on these results with different thermometers and detection methods, we consider that ionomycin locally increases the temperature in HeLa cells on the nanosheets with a high probability, even though ER thermo yellow F.I. was also affected by unknown nonthermal factors.

Based on the present experimental findings, we performed a theoretical calculation assuming a steady-state temperature distribution formed by a cylinder-shaped ER in a cell (Supplemental text, see bottom of PDF). Our calculation revealed that the rate of heat production per unit volume of the ER just proximal to SERCA proteins was 9.4×10^{14} (W/m^3). However, the estimated maximum heat production of the ER by the ATPase proteins is 5.8×10^6 (W/m^3), which is ~10^9 less than the calculated value. Therefore, even if heat production is concentrated at/around the ER in a cell, as reported previously by us (Takei et al., 2014) and others (Yang et al., 2011), calculations simply taking into account the estimated values (i.e., heat production of a SERCA protein and thermal conductivity of the cytoplasm) cannot account for the ionomycin-induced increase in temperature. Therefore, future studies are necessary to experimentally quantify intracellular heat production, thermal conductivity, and other thermal properties, such as thermal diffusivity, relating to unsteady heat conduction, in various types of living cells under activating as well as resting conditions (as discussed in Suzuki et al., 2015b).

Earlier we reported that the surface temperature of HeLa cells is increased by ~1°C upon application of ionomycin, when measured from outside of the cell by using fluorescent microthermometers (Suzuki et al., 2007; compare within ±0.2°C in the present study; see Fig. 3 C). We consider that this apparent inconsistency is due to a difference in the method of temperature measurement: viz., (a) in the previous study (Suzuki et al., 2007), a glass microthermometer was physically pressed on a spherical cell; (b) the cell was, albeit by a small magnitude, deformed by the physical pressure, resulting in the tip of the microthermometer geometrically being wrapped by various intracellular organelles; and (c) close contact to the heat-producing intracellular components, such as the ER, allowed the microthermometer to readily detect a rise in temperature under activating conditions (note that we stated in our previous report that the increase in temperature is dependent upon the area of contact between the microthermometer and the cell; Suzuki et al., 2007). These method steps are in clear contrast to the present method: viz., cells of all types were cultured on the flat surface of the temperature-sensitive RT nanosheets where temperature was measured in a noninvasive manner. In addition, cells of a spherical shape have less of a surface-to-volume ratio (Suzuki et al., 2007) than those of a flat shape (as in the present study), which presumably accumulates a greater amount of internal heat, due to a lesser magnitude of heat loss from the spherical surface.

A rise in cytosolic temperature, if at all, is likely more pronounced in cells in vivo than in those in vitro (i.e., those on nanosheets, as in the present study) because of the following reasons: (a) unlike in cultured conditions, cells are spherical (or cubic) in various organs in vivo, hence they have a smaller surface-to-volume ratio; and (b) while the heat produced in cells on flat nanosheets easily diffuses from the cellular surface to the surrounding medium, and to the coverslip, the higher density of cells in various organs in vivo will prevent the loss of heat. Thus, as the scale of an object is increased, i.e., from single cells to tissues, the magnitude of a rise of temperature in cells will be pronounced accordingly under conditions where heat production per unit volume remains unchanged (as discussed in Baffou et al., 2014). Therefore, the present results with RT nanosheets do not exclude a possible increase in cellular temperature by ~1°C and higher under in vivo conditions. Likewise, thermopiles have been used for external measurement of heat in skeletal and cardiac muscles (Loiselle et al., 2016), and previous studies demonstrated that heat increased in both muscles (thickness, ~1 mm) by ~1m°C upon activation (Daut and Elzinga, 1988; Alpert et al., 1989). It can be assumed that limited thermal diffusion inside preparations with a thickness ~100 times greater than cultured single cells (i.e., ~1 mm versus ~0.01 mm) accounts for the moderate heat production. We consider that the

present thermometry with RT nanosheets is powerful for non-invasive temperature mapping of high-density cellular structures, such as cell sheets, spheroids, and organoids. Furthermore, in order to elucidate the physiological significance of possible heat production in high-density cellular structures, the present thermometry may be used to analyze the temperature-sensing mechanisms at the single cell level, e.g., when heat is applied via IR laser (Tseeb et al., 2009; Itoh et al., 2014; Shintani et al., 2015; Oyama et al., 2015).

In conclusion, we developed a unique form of thermometry with fluorescent thermometer nanosheets enabling measurement/mapping of temperature at the single cell level. We applied the nanosheets to various types of cells, i.e., HeLa cells, HEK293 cells expressing WT or mutated RYR1, brown adipocytes, neonatal cardiomyocytes, and neurons, with the following results: (a) in resting conditions, the temperature difference between the HeLa/HEK293 cells and the medium was within ~0.2°C, and (b) during physiological excitations of cardiomyocytes or neurons, the magnitude of change in the global cellular temperature was within ~0.03°C. Although the temperature at the ER was increased by ~2°C when a large Ca^{2+} burst was induced by ionomycin in HeLa cells, the temperature change was limited just proximal to SERCA proteins, and therefore, the increase in temperature on a global cellular basis was not observed. Likewise, the mitochondrial uncoupler CCCP did not change global temperature for cardiomyocytes or brown adipocytes. These findings support the notion that the heat produced in single cells upon activation does not uniformly increase temperature at the whole cell level; rather, it forms a local temperature gradient just proximal to the heat source, such as SERCA proteins, on the order of ~1°C.

Acknowledgments

Eduardo Ríos served as editor.

We thank Dr. Satoshi Arai (Waseda University; current, Kanazawa University, Kanazawa, Japan) and Dr. Young-Tae Chang (National University of Singapore, Singapore) for provision of ER thermo yellow. We thank Dr. Mari Sato (Hokkaido University, Sapporo, Japan) and Dr. Yu-Hua Tseng (Joslin Diabetes Center/Harvard Medical School, Boston, MA) for provision of WT-1 cells. We thank Ms. Naoko Tomizawa and Ms. Michiyo Murata (The Jikei University School of Medicine) for technical assistance. We thank Dr. Makito Miyazaki (Waseda University; current, Kyoto University, Kyoto, Japan) for critical advice.

This work was supported by Precursory Research for Embryonic Science and Technology (PRESTO), Japan Science and Technology Agency (grant JPMJPR17P3 to K. Oyama), Ministry of Education, Culture, Sports, Science and Technology of Japan Grants-in-Aid for Young Scientists (A) (grant 16H06019 to K. Oyama), Scientific Research on Innovative Areas (grant 23107003 to N. Fukuda), Scientific Research (B) (grant 15H04677 to N. Fukuda), Challenging Exploratory Research (grant 26650053 to K. Oyama and grant 26560225 to N. Fukuda) and the Japan Society for the Promotion of Science Fellows (grant 15J10205 to K. Oyama).

The authors declare no competing financial interests.

Author contributions: K. Oyama, M. Gotoh, T. Yamazawa, S. Ishiwata, and N. Fukuda designed research. K. Oyama, M. Gotoh, Y. Hosaka, T.G. Oyama, A. Kubonoya, Y. Suzuki, S. Tsukamoto, Y. Kawamura, S.A. Shintani, and T. Yamazawa performed experiments. K. Oyama, M. Gotoh, A. Kubonoya., Y. Suzuki, T. Arai, and S.A. Shintani analyzed data. K. Oyama, M. Gotoh, H. Itoh, M. Taguchi, S. Ishiwata, and N. Fukuda interpreted the data. K. Oyama, M. Gotoh, S. Ishiwata, and N. Fukuda drafted the manuscript. All authors have approved the final draft of the manuscript, and their contributions qualify them as authors.

Submitted: 22 August 2019
Accepted: 17 April 2020

References

Albe, K.R., M.H. Butler, and B.E. Wright. 1990. Cellular concentrations of enzymes and their substrates. *J. Theor. Biol.* 143:163–195. https://doi.org/10.1016/S0022-5193(05)80266-8

Alberts, B., A. Johnson, J. Lewis, M. Raff, K. Roberts, and P. Walter. 2008. Molecular Biology of the Cell. Fifth edition. Garland Science, New York. 697 pp.

Alpert, N.R., E.M. Blanchard, and L.A. Mulieri. 1989. Tension-independent heat in rabbit papillary muscle. *J. Physiol.* 414:433–453. https://doi.org/10.1113/jphysiol.1989.sp017697

Arai, S., S.-C. Lee, D. Zhai, M. Suzuki, and Y.T. Chang. 2014. A molecular fluorescent probe for targeted visualization of temperature at the endoplasmic reticulum. *Sci. Rep.* 4:6701. https://doi.org/10.1038/srep06701

Arai, S., M. Suzuki, S.-J. Park, J.S. Yoo, L. Wang, N.-Y. Kang, H.-H. Ha, and Y.-T. Chang. 2015. Mitochondria-targeted fluorescent thermometer monitors intracellular temperature gradient. *Chem. Commun. (Camb.).* 51:8044–8047. https://doi.org/10.1039/C5CC01088H

Baffou, G., H. Rigneault, D. Marguet, and L. Jullien. 2014. A critique of methods for temperature imaging in single cells. *Nat. Methods.* 11:899–901. https://doi.org/10.1038/nmeth.3073

Curtis, A.S.G.. 1964. The mechanism of adhesion of cells to glass. A study by interference reflection microscopy. *J. Cell Biol.* 20:199–215. https://doi.org/10.1083/jcb.20.2.199

Daut, J., and G. Elzinga. 1988. Heat production of quiescent ventricular trabeculae isolated from guinea-pig heart. *J. Physiol.* 398:259–275. https://doi.org/10.1113/jphysiol.1988.sp017041

Ellis, R.J.. 2001. Macromolecular crowding: an important but neglected aspect of the intracellular environment. *Curr. Opin. Struct. Biol.* 11:114–119. https://doi.org/10.1016/S0959-440X(00)00172-X

Else, P.L., and A.J. Hulbert. 1985. An allometric comparison of the mitochondria of mammalian and reptilian tissues: the implications for the evolution of endothermy. *J. Comp. Physiol. B.* 156:3–11. https://doi.org/10.1007/BF00692920

Gota, C., K. Okabe, T. Funatsu, Y. Harada, and S. Uchiyama. 2009. Hydrophilic fluorescent nanogel thermometer for intracellular thermometry. *J. Am. Chem. Soc.* 131:2766–2767. https://doi.org/10.1021/ja807714j

Inomata, N., M. Toda, M. Sato, A. Ishijima, and T. Ono. 2012. Pico calorimeter for detection of heat produced in an individual brown fat cell. *Appl. Phys. Lett.* 100. 154104. https://doi.org/10.1063/1.3701720

Inomata, N., M. Toda, and T. Ono. 2016. Highly sensitive thermometer using a vacuum-packed Si resonator in a microfluidic chip for the thermal measurement of single cells. *Lab Chip.* 16:3597–3603. https://doi.org/10.1039/C6LC00949B

Ishii, S., K. Oyama, T. Arai, H. Itoh, S.A. Shintani, M. Suzuki, F. Kobirumaki-Shimozawa, T. Terui, N. Fukuda, and S. Ishiwata. 2019. Microscopic heat pulses activate cardiac thin filaments. *J. Gen. Physiol.* 151:860–869. https://doi.org/10.1085/jgp.201812243

Itoh, H., K. Oyama, M. Suzuki, and S. Ishiwata. 2014. Microscopic heat pulse-induced calcium dynamics in single WI-38 fibroblasts. *Biophysics.* 10:109–119. https://doi.org/10.2142/biophysics.10.109

Itoh, H., S. Arai, T. Sudhaharan, S.-C. Lee, Y.-T. Chang, S. Ishiwata, M. Suzuki, and E.B. Lane. 2016. Direct organelle thermometry with fluorescence lifetime imaging microscopy in single myotubes. *Chem. Commun. (Camb.).* 52:4458–4461. https://doi.org/10.1039/C5CC09943A

Kiyonaka, S., T. Kajimoto, R. Sakaguchi, D. Shinmi, M. Omatsu-Kanbe, H. Matsuura, H. Imamura, T. Yoshizaki, I. Hamachi, T. Morii, et al. 2013. Genetically encoded fluorescent thermosensors visualize subcellular thermoregulation in living cells. *Nat. Methods*. 10:1232–1238. https://doi.org/10.1038/nmeth.2690

Kolodner, P., and J.A. Tyson. 1982. Microscopic fluorescent imaging of surface temperature profiles with 0.01°C resolution. *Appl. Phys. Lett*. 40: 782–784. https://doi.org/10.1063/1.93258

Kriszt, R., S. Arai, H. Itoh, M.H. Lee, A.G. Goralczyk, X.M. Ang, A.M. Cypess, A.P. White, F. Shamsi, R. Xue, et al. 2017. Optical visualisation of thermogenesis in stimulated single-cell brown adipocytes. *Sci. Rep*. 7: 1383. https://doi.org/10.1038/s41598-017-00291-9

Loiselle, D.S., C.M. Johnston, J.-C. Han, P.M.F. Nielsen, and A.J. Taberner. 2016. Muscle heat: a window into the thermodynamics of a molecular machine. *Am. J. Physiol. Heart Circ. Physiol*. 310:H311–H325. https://doi.org/10.1152/ajpheart.00569.2015

Milo, R.. 2013. What is the total number of protein molecules per cell volume? A call to rethink some published values. *BioEssays*. 35:1050–1055. https://doi.org/10.1002/bies.201300066

Murayama, T., N. Kurebayashi, T. Yamazawa, H. Oyamada, J. Suzuki, K. Kanemaru, K. Oguchi, M. Iino, and T. Sakurai. 2015. Divergent activity profiles of type 1 ryanodine receptor channels carrying malignant hyperthermia and central core disease mutations in the amino-terminal region. *PLoS One*. 10. e0130606. https://doi.org/10.1371/journal.pone.0130606

Nakano, M., Y. Arai, I. Kotera, K. Okabe, Y. Kamei, and T. Nagai. 2017. Genetically encoded ratiometric fluorescent thermometer with wide range and rapid response. *PLoS One*. 12. e0172344. https://doi.org/10.1371/journal.pone.0172344

Nguyen, K.H., S. Mishra, and B.L. Nyomba. 2015. In vitro differentiation of mouse brown preadipocytes is enhanced by IGFBP-3 expression and reduced by IGFBP-3 silencing. *Obesity (Silver Spring)*. 23:2083–2092. https://doi.org/10.1002/oby.21204

Okabe, K., N. Inada, C. Gota, Y. Harada, T. Funatsu, and S. Uchiyama. 2012. Intracellular temperature mapping with a fluorescent polymeric thermometer and fluorescence lifetime imaging microscopy. *Nat. Commun*. 3:705. https://doi.org/10.1038/ncomms1714

Okabe, K., R. Sakaguchi, B. Shi, and S. Kiyonaka. 2018. Intracellular thermometry with fluorescent sensors for thermal biology. *Pflugers Arch*. 470:717–731. https://doi.org/10.1007/s00424-018-2113-4

Oyama, K., V. Zeeb, Y. Kawamura, T. Arai, M. Gotoh, H. Itoh, T. Itabashi, M. Suzuki, and S. Ishiwata. 2015. Triggering of high-speed neurite outgrowth using an optical microheater. *Sci. Rep*. 5:16611. https://doi.org/10.1038/srep16611

Sato, M.K., M. Toda, N. Inomata, H. Maruyama, Y. Okamatsu-Ogura, F. Arai, T. Ono, A. Ishijima, and Y. Inoue. 2014. Temperature changes in brown adipocytes detected with a bimaterial microcantilever. *Biophys. J*. 106: 2458–2464. https://doi.org/10.1016/j.bpj.2014.04.044

Schwarz, D.S., and M.D. Blower. 2016. The endoplasmic reticulum: structure, function and response to cellular signaling. *Cell. Mol. Life Sci*. 73:79–94. https://doi.org/10.1007/s00018-015-2052-6

Sekiguchi, T., S. Sotoma, and Y. Harada. 2018. Fluorescent nanodiamonds as a robust temperature sensor inside a single cell. *Biophys. Physicobiol*. 15: 229–234. https://doi.org/10.2142/biophysico.15.0_229

Shintani, S.A., K. Oyama, F. Kobirumaki-Shimozawa, T. Ohki, S. Ishiwata, and N. Fukuda. 2014. Sarcomere length nanometry in rat neonatal cardiomyocytes expressed with α-actinin-AcGFP in Z discs. *J. Gen. Physiol*. 143:513–524. https://doi.org/10.1085/jgp.201311118

Shintani, S.A., K. Oyama, N. Fukuda, and S. Ishiwata. 2015. High-frequency sarcomeric auto-oscillations induced by heating in living neonatal cardiomyocytes of the rat. *Biochem. Biophys. Res. Commun*. 457:165–170. https://doi.org/10.1016/j.bbrc.2014.12.077

Suzuki, M., V. Tseeb, K. Oyama, and S. Ishiwata. 2007. Microscopic detection of thermogenesis in a single HeLa cell. *Biophys. J*. 92:L46–L48. https://doi.org/10.1529/biophysj.106.098673

Suzuki, M., S. Arai, K. Oyama, and S. Ishiwata. 2015a. Luminescent Nanothermometers for Biological Applications. *In* CRC Concise Encyclopedia of Nanotechnology. B.I. Kharisov, O.V. Kharissova, and U. Ortiz-Mendez, editors. CRC Press, Boca Raton, FL. 851–859.

Suzuki, M., V. Zeeb, S. Arai, K. Oyama, and S. Ishiwata. 2015b. The 10(5) gap issue between calculation and measurement in single-cell thermometry. *Nat. Methods*. 12:802–803. https://doi.org/10.1038/nmeth.3551

Takei, Y., S. Arai, A. Murata, M. Takabayashi, K. Oyama, S. Ishiwata, S. Takeoka, and M. Suzuki. 2014. A nanoparticle-based ratiometric and self-calibrated fluorescent thermometer for single living cells. *ACS Nano*. 8:198–206. https://doi.org/10.1021/nn405456e

Tanimoto, R., T. Hiraiwa, Y. Nakai, Y. Shindo, K. Oka, N. Hiroi, and A. Funahashi. 2016. Detection of temperature difference in neuronal cells. *Sci. Rep*. 6:22071. https://doi.org/10.1038/srep22071

Tseeb, V., M. Suzuki, K. Oyama, K. Iwai, and S. Ishiwata. 2009. Highly thermosensitive Ca dynamics in a HeLa cell through IP^3 receptors. *HFSP J*. 3:117–123. https://doi.org/10.2976/1.3073779

Tsukamoto, S., T. Fujii, K. Oyama, S.A. Shintani, T. Shimozawa, F. Kobirumaki-Shimozawa, S. Ishiwata, and N. Fukuda. 2016. Simultaneous imaging of local calcium and single sarcomere length in rat neonatal cardiomyocytes using yellow Cameleon-Nano140. *J. Gen. Physiol*. 148: 341–355. https://doi.org/10.1085/jgp.201611604

Uchiyama, S., C. Gota, T. Tsuji, and N. Inada. 2017. Intracellular temperature measurements with fluorescent polymeric thermometers. *Chem. Commun. (Camb.)*. 53:10976–10992. https://doi.org/10.1039/C7CC06203F

Verschueren, H.. 1985. Interference reflection microscopy in cell biology: methodology and applications. *J. Cell Sci*. 75:279–301.

Wang, C., R. Xu, W. Tian, X. Jiang, Z. Cui, M. Wang, H. Sun, K. Fang, and N. Gu. 2011. Determining intracellular temperature at single-cell level by a novel thermocouple method. *Cell Res*. 21:1517–1519. https://doi.org/10.1038/cr.2011.117

Yamada, T., N. Inomata, and T. Ono. 2016. Sensitive thermal microsensor with pn junction for heat measurement of a single cell. *Jpn. J. Appl. Phys*. 55. 027001. https://doi.org/10.7567/JJAP.55.027001

Yang, J.-M., H. Yang, and L. Lin. 2011. Quantum dot nano thermometers reveal heterogeneous local thermogenesis in living cells. *ACS Nano*. 5: 5067–5071. https://doi.org/10.1021/nn201142f

Yang, F., G. Li, J. Yang, Z. Wang, D. Han, F. Zheng, and S. Xu. 2017. Measurement of local temperature increments induced by cultured HepG2 cells with micro-thermocouples in a thermally stabilized system. *Sci. Rep*. 7:1721. https://doi.org/10.1038/s41598-017-01891-1

Zeeb, V., M. Suzuki, and S. Ishiwata. 2004. A novel method of thermal activation and temperature measurement in the microscopic region around single living cells. *J. Neurosci. Methods*. 139:69–77. https://doi.org/10.1016/j.jneumeth.2004.04.010

Zohar, O., M. Ikeda, H. Shinagawa, H. Inoue, H. Nakamura, D. Elbaum, D.L. Alkon, and T. Yoshioka. 1998. Thermal imaging of receptor-activated heat production in single cells. *Biophys. J*. 74:82–89. https://doi.org/10.1016/S0006-3495(98)77769-0

Supplemental material

Supplemental methods

Time-lapse imaging and live/dead assay of HeLa cells on RT nanosheets

HeLa cells in culture medium were placed on RT nanosheets and immediately mounted on a sample stage of a fluorescence microscope BZ-9000 (Keyence). After incubation for 30 min for stabilization of temperature, phase-contrast, time-lapse images were captured at intervals of 5 min at 37°C with 5% CO_2. The objective lens used for this experiment was Plan Fluor ELWD 20×/0.45 (Nikon).

In live/dead assays (Fig. S5), HeLa cells were cultured on RT nanosheets or glass bottom culture dishes for 3 d. Then, 0.5 µM Calcein-AM and 0.5 µg/ml DAPI (4′,6-diamidino-2-phenylindole; Dojindo Laboratories) were added to the 2-ml culture medium. After incubation for 30 min at 37°C with 5% CO_2, the cells were observed by BZ-9000 at 37°C with 5% CO_2. An objective lens Plan Fluor ELWD 20×/0.45 (Nikon) was used. An excitation filter, a dichroic mirror, and an emission filter for the observation of Calcein were 470/40, 495, and 535/50 nm, respectively. An excitation filter, a dichroic mirror, and an emission filter for DAPI were 360/40, 400, and 460/50 nm, respectively. These mirrors/filters were purchased from Chroma Technology. Viability was calculated from the number of Calcein-positive cells divided by the number of total cells.

Temperature measurement for HEK293 expressing mutant RYR1

HEK293 cells encoding rabbit skeletal muscle RYR1 or the mutants (R164C or Y523S) were generated as described previously (Murayama et al., 2015). The expression of RYR1s was elicited by using the Flp-In T-REx system (Thermo Fisher Scientific). The HEK293 cells were cultured on collagen-coated culture dishes (TPP Techno Plastic Products) in the culture medium (DMEM containing 10% FBS, 2 mM L-glutamine, 100 U/ml penicillin, and 100 µg/ml streptomycin) containing 100 µg/ml hygromycin and 15 µg/ml blasticidin (InvivoGen) at 37°C with 5% CO_2. The dishes were pre-coated with 0.001% collagen type 1 (Research Institute for the Functional Peptides) diluted in sterilized, distilled water for 1 h at 37°C, and washed with the culture medium just prior to cell culture. L-glutamine and hygromycin were purchased from Nacalai Tesque. 2 d before experiments, cells were seeded on collagen-coated RT nanosheets, as described above. To induce expression of RYR1, the culture medium was changed to the culture medium containing 2 µg/ml doxycycline (Sigma-Aldrich, Merck), and the cells were observed 24–30 h after induction. Experimental conditions (i.e., microscope, solution, and procedures) for temperature imaging with RT nanosheets were the same as those used for HeLa cells. For control cells, we used cells encoding WT RYR1 without induction.

For immunostaining of RYR1, cells on RT nanosheets 1 d after induction were fixed, in the way used for HeLa cells. After washing with PBS, the fixed cells were incubated in blocking solution (PBS containing 1% BSA; Biowest) for 60 min at room temperature. After blocking, cells were incubated in blocking solution containing mouse RYR1 monoclonal antibody (34C; 1:300, MA3-925, Thermo Fisher Scientific) for 60 min at room temperature. After washing with blocking solution, cells were incubated in blocking solution containing Alexa Fluor 488–conjugated anti-mouse IgG (1:300, A-11001, Thermo Fisher Scientific) for 60 min at room temperature. Cells were then washed with PBS and incubated in PBS containing 1 µg/ml DAPI for 10 min at room temperature. Cells in fresh PBS were observed by BZ-9000. The objective lens used for this experiment was Plan Fluor 40×/0.75 (Nikon). The excitation filter, dichroic mirror, and emission filter for Alexa Fluor 488 were 470/40, 495, and 535/50 nm, respectively. The excitation filter, dichroic mirror, and emission filter for DAPI were 360/40, 400, and 460/50, respectively. These mirrors/filters were from Chroma Technology.

Temperature measurement for mitochondrial thermogenesis

Rat neonatal cardiomyocytes were cultured on collagen-coated RT nanosheets (5 mg/ml EuTTA, 2.5 µg/ml Rh101, and 10 mg/ml PMMA) in DMEM containing 4 mM L-glutamine (Sigma-Aldrich), 1 mM sodium pyruvate (Sigma-Aldrich), 10% FBS, 100 U/ml penicillin, and 100 µg/ml streptomycin at 37°C with 5% CO_2. At 4–5 d in vitro, cardiomyocytes on RT nanosheets were incubated in 1.9 ml of 1.8 mM Ca^{2+}-HEPES-Tyrode's solution, mounted on a sample stage and observed at 37°C under a microscope. For temperature imaging of the SR, cardiomyocytes on collagen-coated glass bottom dishes were incubated in 1.8 mM Ca^{2+}-HEPES-Tyrode's solution containing 100 nM ER thermo yellow and 1 µM ER tracker green (Thermo Fisher Scientific) for 30 min at 37°C with 5% CO_2. To inhibit mitochondrial activities, cardiomyocytes stained with both ER thermo yellow and ER tracker green were incubated in 1.8 mM Ca^{2+}-HEPES-Tyrode's solution containing 10 µM rotenone (0.1% DMSO) for 30 min prior to the observation. After the onset of observation, 100 µl of 1.8 mM Ca^{2+}-HEPES-Tyrode's solution containing 200 µM CCCP (Sigma-Aldrich; 2% DMSO) or 2% DMSO was applied at ~10 mm from the observed cells. Non-beating cells before stimulation, due presumably to unhealthiness, contamination of fibroblasts, or both, were excluded from the analysis.

WT-1 cells were cultured on collagen-coated RT nanosheets (5 mg/ml EuTTA, 2.5 µg/ml Rh101, and 10 mg/ml PMMA) in DMEM containing 2 mM L-glutamine (Sigma-Aldrich), 10% FBS, 100 U/ml penicillin, and 100 µg/ml streptomycin at 37°C with 5% CO_2.

After reaching confluency, the medium was changed to DMEM containing 2 mM L-glutamine, 2% FBS, 100 U/ml penicillin and 100 μg/ml streptomycin, 500 μM 3-isobutyl-1-methylxanthine (IBMX; Nacalai Tesque), 125 μM indomethacin (FUJIFILM Wako Pure Chemical), 5 μM dexamethasone (FUJIFILM Wako Pure Chemical), 20 nM insulin (Sigma-Aldrich), and 1 nM 3,3′,5-Triiodo-L-thyronine (T_3; Sigma-Aldrich). After 2 d, the medium was changed to DMEM containing 2 mM L-glutamine, 2% FBS, 100 U/ml penicillin and 100 μg/ml streptomycin, 20 nM insulin, and 1 nM T_3 and cultured for 3–5 d before measurement. The medium was changed every 1–2 d.

Brown preadipocytes were obtained from male 3-wk-old ICR mice. Interscapular brown adipose tissue in an isolation buffer (123 mM NaCl, 5mK KCl, 1.3 mM $CaCl_2$, 5 mM glucose, 2% BSA, and 100 mM HEPES, pH 7.4 with NaOH) was minced and incubated in an isolation buffer containing 1.5 mg/ml collagenase (FUJIFILM Wako Pure Chemical) for 30 min at 37°C (Nguyen et al., 2015). The tissue was filtered through a 200-μm filter (pluriStrainer, pluriSelect Life Science) and centrifuged at 200 g for 5 min. Preadipocytes in the pellet were cultured on a 10-cm dish (Corning) in DMEM containing 2 mM L-glutamine (Sigma-Aldrich), 10% FBS, 100 U/ml penicillin, and 100 μg/ml streptomycin for 4–5 d with daily medium change. The cells were trypsinized and cultured on collagen-coated RT nanosheets or glass bottom dishes. After reaching confluent, the medium was changed to DMEM containing 2 mM L-glutamine, 10% FBS, 100 U/ml penicillin and 100 μg/ml streptomycin, 500 μM IBMX, 125 μM indomethacin, 5 μM dexamethasone, 20 nM insulin, and 1 nM T_3. After 2 d, the medium was changed to DMEM containing 2 mM L-glutamine, 10% FBS, 100 U/ml penicillin and 100 μg/ml streptomycin, 20 nM insulin, and 1 nM T_3 and cultured for 3–5 d before the measurement. The medium was changed every 1–2 d.

WT-1 adipocytes and mouse brown adipocytes on collagen-coated RT nanosheets were incubated in 1.9 ml of HBSS (1.8 mM $CaCl_2$), mounted on a sample stage and observed at 37°C under a microscope. For temperature imaging of the ER, adipocytes on collagen-coated glass bottom dishes were incubated in HBSS containing 100 nM ER thermo yellow and 1 μM ER tracker green for 30 min at 37°C with 5% CO_2. To inhibit mitochondrial activities, WT-1 adipocytes stained with both ER thermo yellow and ER tracker green were incubated in HBSS containing 10 μM rotenone (0.1% DMSO) for 30 min before observation. After the onset of observation, 100 μl of HBSS containing 200 μM CCCP (2% DMSO) or 2% DMSO was applied at ~10 mm from the observed cells.

In experiments with cardiomyocytes or adipocytes, RT nanosheets (5 mg/ml EuTTA, 2.5 μg/ml Rh101, and 10 mg/ml PMMA) were hydrophilized with a vacuum plasma device (YHS-R; SAKIGAKE-Semiconductor). The nanosheets or glass bottom dishes were coated with 0.3 mg/ml collagen (Cellmatrix Type I-C, Nitta Gelatin) diluted in 1 mM HCl and incubated for 5 min at room temperature. An inverted microscope (IX-83, Olympus) equipped with an EMCCD camera (iXon Life 888, Andor Technology) was used for fluorescence measurement. RT nanosheets and other fluorescent dyes were excited by a 4-wavelength high-power LED source (LED4D237, 365/490/565/660 nm, Thorlabs), and observed by a PlanApo N 60×/1.45 oil immersion objective lens (Olympus). The excitation filters BP360-370 (Olympus), FF01-469/35 (Semrock), and FF01-554/23 (Semrock) were used for EuTTA, ER tracker green, and Rh101 and ER thermo yellow, respectively. A dichroic mirror FF493/574-Di01 (Semrock) and an emission filter FF01-512/630 (Semrock) were also used. The excitation light was changed using an optical filter changer Lambda 10-b (Sutter Instrument). The local temperature was increased by irradiation with an IR laser (λ = 1,475 nm, AF4B150FK75L, Anritsu).

Supplemental Discussion

Theoretical calculation on temperature distribution by the ER in a cell

In the present study, we calculated the steady-state temperature distribution created by a cylinder-shaped ER. The rate of heat generation per unit volume q is described as:

$$q = \frac{2\kappa}{r_1^2 \ln\left(\frac{r_2}{r_1}\right)}(T_1 - T_2)$$

where r_1 denotes the radius of the cylinder, r_2 the distance from the center of the heat source, κ thermal conductivity, T_1 the temperature at the distance r_1 (i.e., the surface temperature of the cylinder), and T_2 the temperature at the distance r_2. We assumed that (a) r_1 equals 25 nm (cf. Schwarz and Blower, 2016), (b) the distance between the ER and a thermometer nanosheet (r_2) is 1 μm, (c) the averaged thermal conductivity of the region between the ER and the nanosheet is the same as water (i.e., 0.6 W/m/K) and (d) the difference between T_1 and T_2 is >1.8 K (cf. Fig. 3). Accordingly, q is derived as 9.4×10^{14} (W/m^3). We previously calculated that the estimated maximum heat production of SERCA proteins in the cytoplasm is 8.7×10^5 (W/m^3; Takei et al., 2014). Assuming that the ER/cytosol volume ratio is 0.15 (Alberts et al., 2008), the rate of heat generation per unit volume in the ER is 5.8×10^6 (W/m^3), which is ~10^9 smaller than the value of q calculated above (i.e., 9.4×10^{14} [W/m^3]).

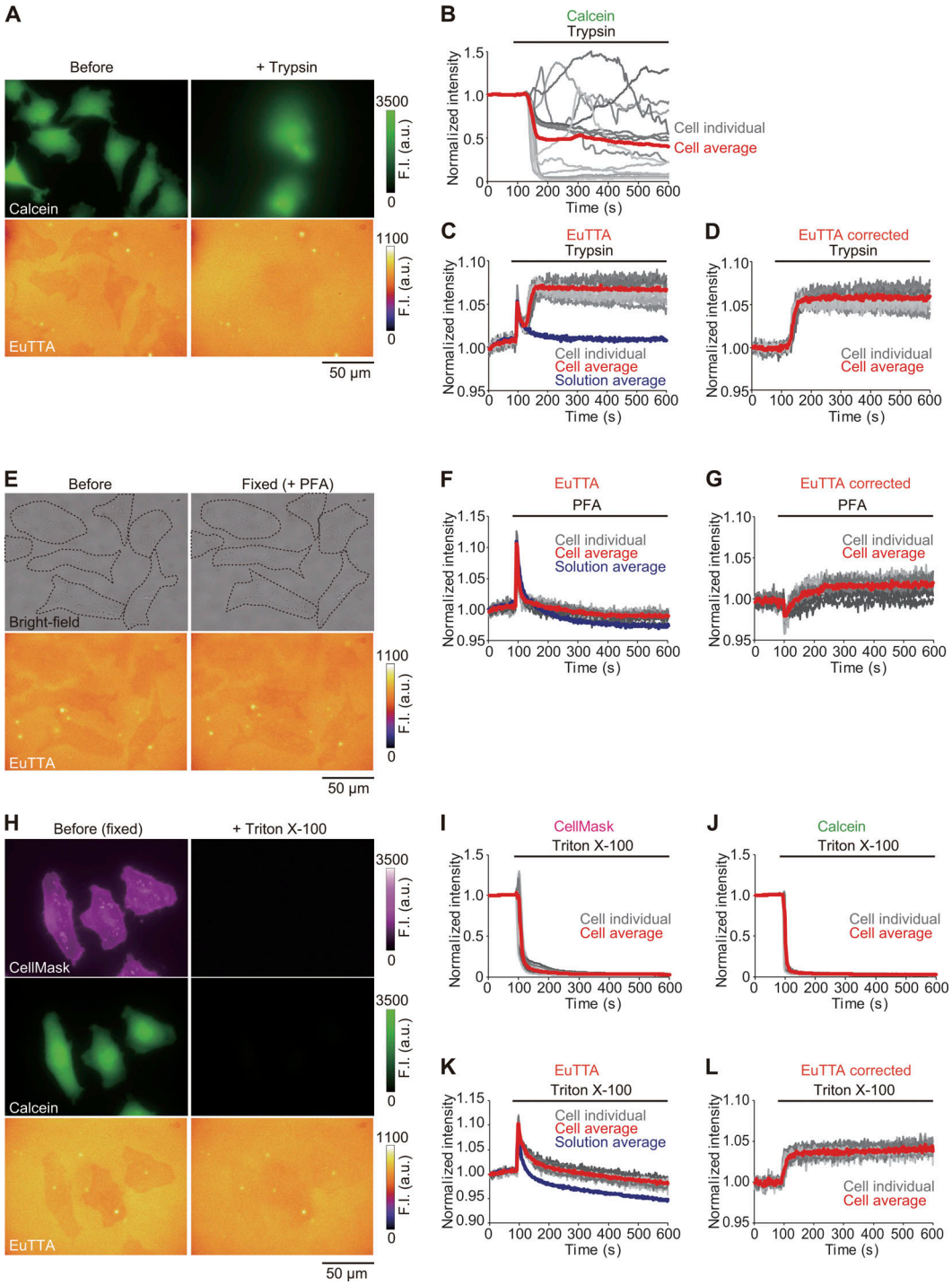

Figure S1. **Changes in the F.I. of EuTTA nanosheets with HeLa cells before and after treatment with trypsin, PFA, or Triton X-100. (A)** Top: Fluorescence images of Calcein in HeLa cells on the EuTTA nanosheet before (left) and after (right) 0.12% trypsin treatment. Bottom: Fluorescence images of the EuTTA nanosheet. See Video 1. **(B)** Time course of changes in Calcein F.I. in HeLa cells during trypsin treatment. Gray, individual cells; red, average. **(C)** Same as in B for EuTTA F.I. Gray, individual cells; red, average with cells; blue, average without cells (i.e., average for solution). **(D)** Same as in C for the corrected F.I. of the EuTTA nanosheet (see Materials and methods for details). Gray, individual cells; red, average. In B, C, and D, trypsin is present during the period shown by the horizontal black line on top of each graph (applied at 90 s). Number of cells, 15 (n = 3). **(E)** Top: Bright-field images of HeLa cells on the EuTTA nanosheet before (left) and after fixation with 4% PFA (right). Bottom: Fluorescence images of the EuTTA nanosheet. **(F and G)** Same as in C and D, respectively, but with PFA. In F and G, PFA is present during the period indicated by the horizontal black line on top of each graph (applied at 90 s). Number of cells, 11 (n = 2). **(H)** Top: Fluorescence images of CellMask in chemically fixed HeLa cells on the EuTTA nanosheet before (left) and after (right) treatment with 0.9% (vol/vol) Triton X-100. Middle: Same as in top for fluorescence images of Calcein. Bottom: Same as in top for fluorescence images of the EuTTA nanosheet. See Video 2. **(I)** Time course of changes in the F.I. of CellMask in chemically fixed HeLa cells on the EuTTA nanosheet during treatment with Triton X-100. **(J)** Same as in I for Calcein. **(K and L)** Same as in C and D but during Triton X-100 treatment. In I–L, the horizontal black line indicates the period of Triton X-100 treatment. Number of cells, 13 (n = 3). The fluorescence images were averaged from 30 frames before (0–58 s) and after treatment (540–598 s).

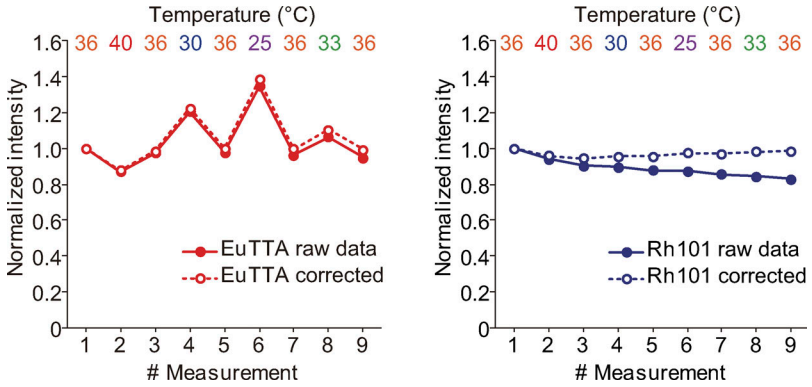

Figure S2. **Temperature sensitivity of EuTTA or Rh101 of a RT nanosheet.** Time course of changes in EuTTA (left) or Rh101 (right) F.I. Temperature is shown on top of each graph. Closed circle and solid line, raw data; open circle and dashed line, corrected data. In both graphs, F.I. is normalized by that obtained at the first measurement. See Materials and methods for details.

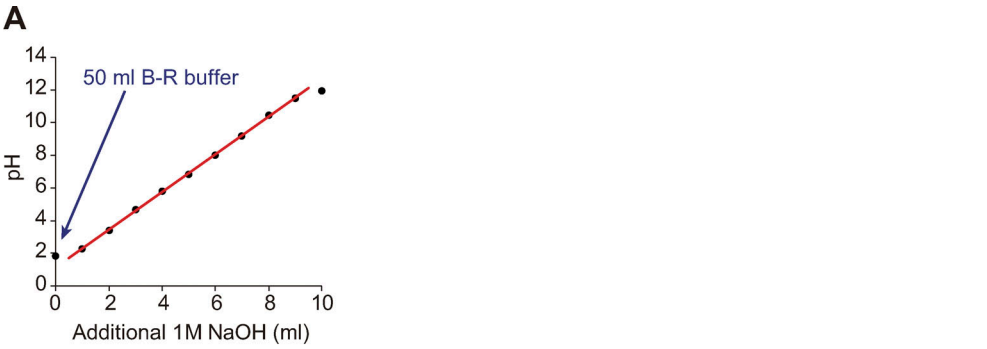

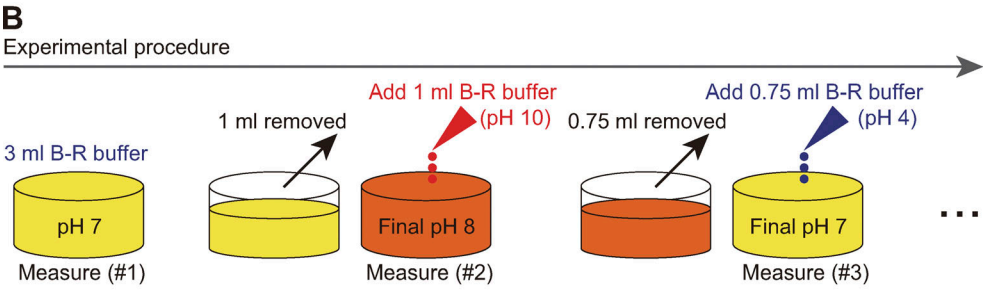

# Measurement	1	2	3	4	5	6	7	8	9
Exchanged volume (ml)		1	0.75	1	0.75	2	1.2	2	1.2
pH (added B-R buffer)		10	4	4	10	4	10	10	4
pH (final)	7	8	7	6	7	5	7	9	7

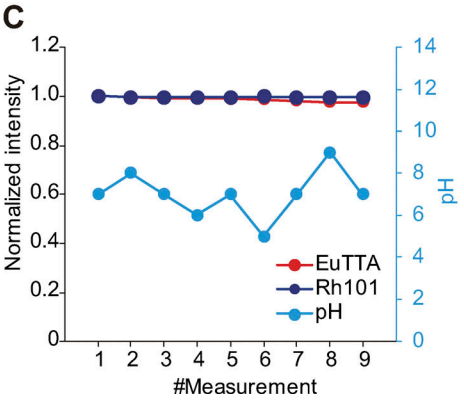

Figure S3. **Stability of RT nanosheets at various pH. (A)** Changes in pH in B–R buffer (40 mM H_3BO_3, 40 mM H_3PO_4, and 40 mM CH_3COOH) when 1 M NaOH was applied to 50 ml of the buffer. pH was changed linearly with the volume of added NaOH. The linear pH-buffering characteristics enabled us to adjust pH in the experiment in B. **(B)** Illustration showing an experimental procedure for F.I. measurement of RT nanosheets at various pH levels. See Materials and methods for details. **(C)** Graph showing the F.I. of EuTTA (red) or Rh101 (blue) of a RT nanosheet at various pH (cyan blue). Red circles with a red line, EuTTA; blue circles with a blue line, Rh101; cyan blue circles with a cyan blue line, pH. F.I. for EuTTA or Rh101 was normalized by that obtained at the first measurement.

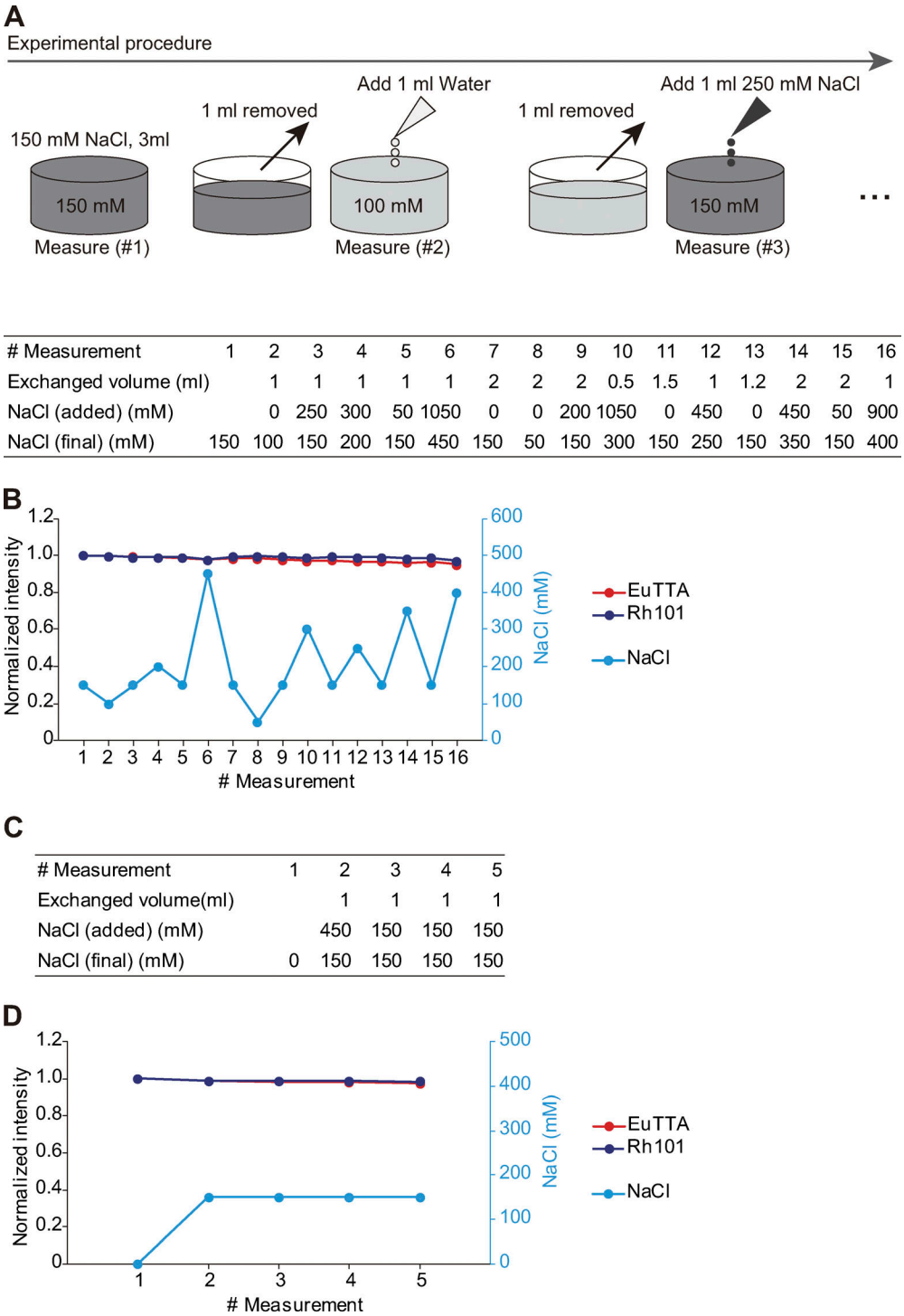

# Measurement	1	2	3	4	5	6	7	8	9	10	11	12	13	14	15	16
Exchanged volume (ml)		1	1	1	1	1	2	2	2	0.5	1.5	1	1.2	2	2	1
NaCl (added) (mM)		0	250	300	50	1050	0	0	200	1050	0	450	0	450	50	900
NaCl (final) (mM)	150	100	150	200	150	450	150	50	150	300	150	250	150	350	150	400

# Measurement	1	2	3	4	5
Exchanged volume(ml)		1	1	1	1
NaCl (added) (mM)		450	150	150	150
NaCl (final) (mM)	0	150	150	150	150

Figure S4. **Stability of RT nanosheets at various ionic strengths. (A)** Illustration showing an experimental procedure for measurement of the F.I. of RT nanosheets at various ionic strengths. Ionic strength was adjusted by NaCl. See Materials and methods for details. **(B)** Graph showing the F.I. of EuTTA (red) or Rh101 (blue) of a RT nanosheet at various ionic strengths (cyan blue). Red circles with a red line, EuTTA; blue circles with a blue line, Rh101; cyan blue circles with a cyan blue line, ionic strength. F.I. was normalized by that obtained at the first measurement. **(C and D)** Same as in A and B, respectively, but the first measurement was conducted in distilled water.

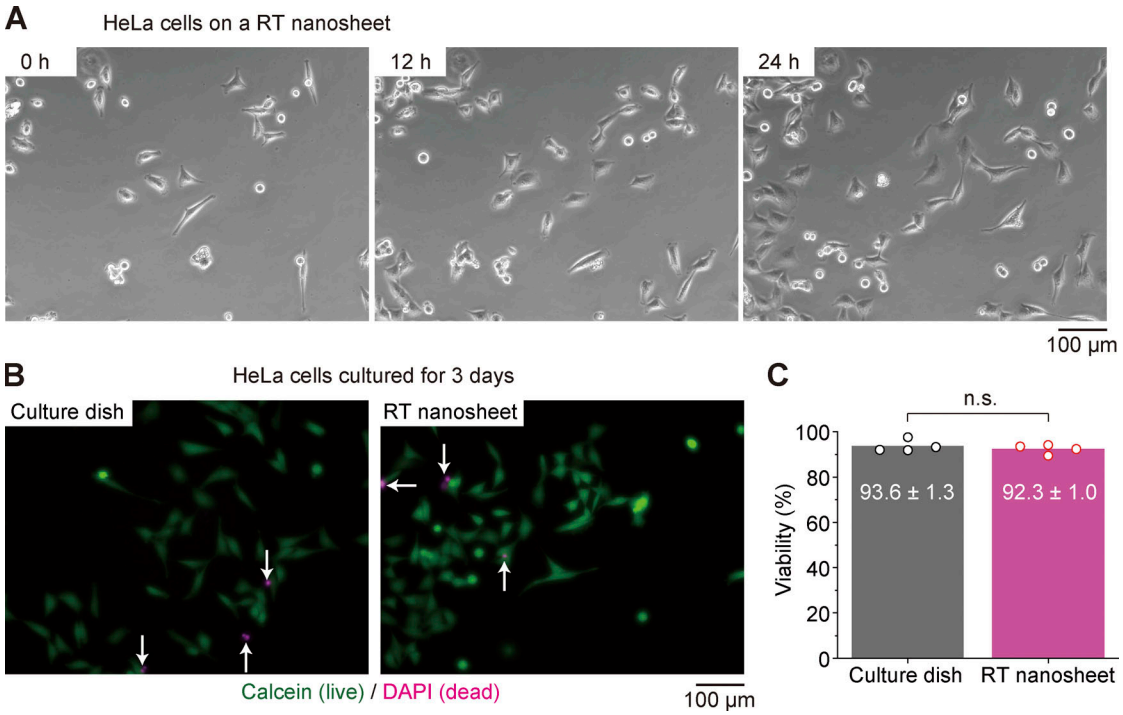

Figure S5. **Culture of HeLa cells on RT nanosheets. (A)** Time-lapse phase-contrast images of HeLa cells on a RT nanosheet. Images at the onset of culture (left), and at 12 (middle) and 24 h (right) are shown. See Video 3. **(B)** Live/dead assay for HeLa cells on a culture dish (left) and a RT nanosheet (right) after the 3-d culture. Fluorescence of Calcein and that of DAPI (white arrows) indicate live and dead cells, respectively. **(C)** Comparison of variability of HeLa cells cultured on culture dishes (gray) and RT nanosheets (pink). Number of cells, 1,453 and 1,420 on culture dishes and RT nanosheets, respectively. n = 4. The Mann–Whitney U test was performed. n.s., not significant.

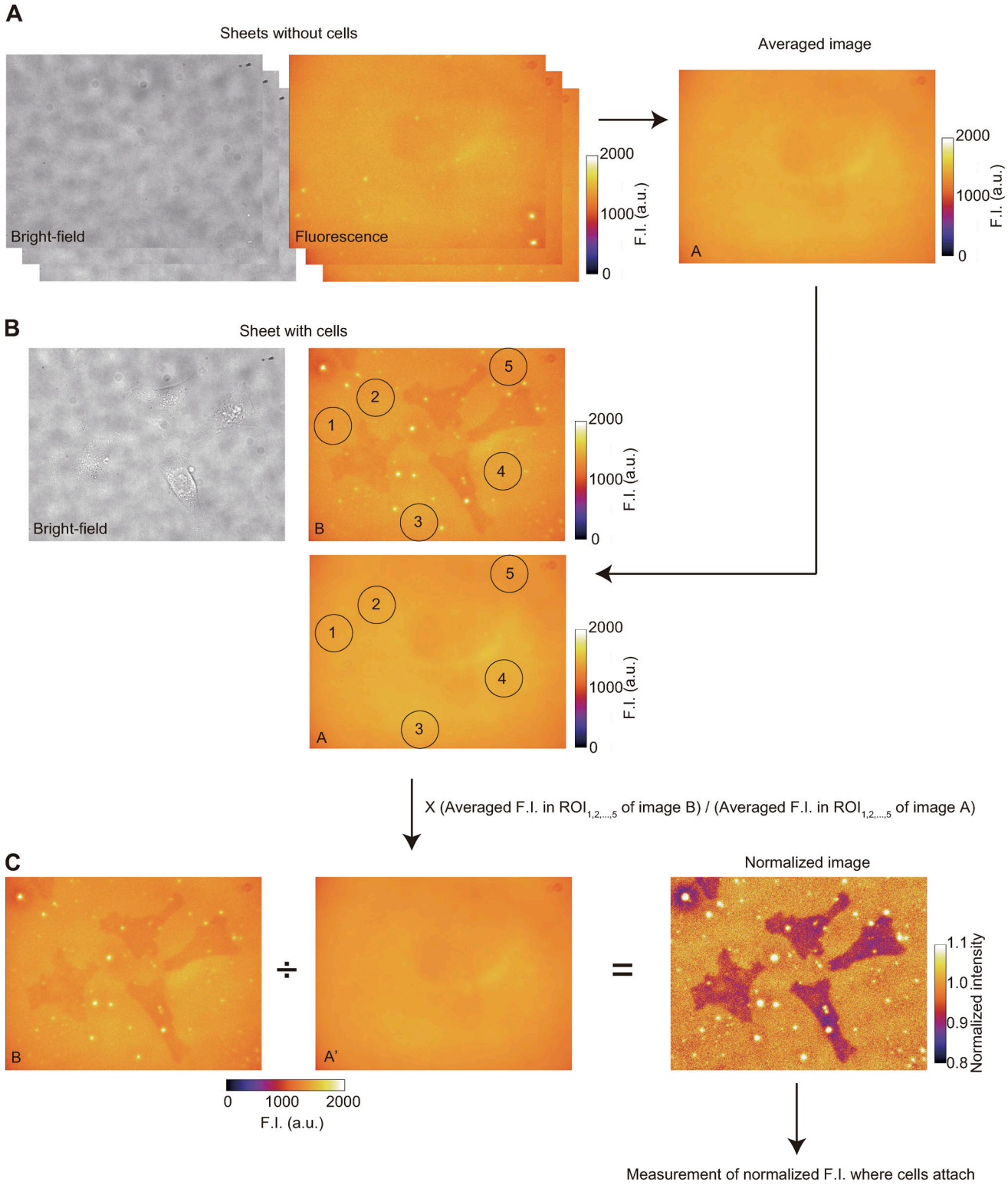

Figure S6. **Normalization procedure for fluorescence images of RT nanosheets. (A)** Bright-field (left) and fluorescence (right) images of RT nanosheets without cells. Fluorescence images of RT nanosheets without cells were averaged. The averaged image (image A, right) shows uniformity of the excitation light. **(B)** Top left: Bright-field image of HeLa cells on a RT nanosheet. Top right: Fluorescence image of the RT nanosheet in top left (image B). F.I. of image B in five regions of interest (ROIs) without cells was measured. F.I. of image A in the same five ROIs was also measured. **(C)** Image B (left) was divided by image A' (middle) which had been obtained by adjusting the intensity of image A; hence each F.I. of five ROIs in image A' was equal to that in image B. Therefore, the "normalized image" (right) shows the darkness of the RT nanosheet on which cells were present. The normalized images and their intensities with cells are shown in Fig. 2 and Fig. S8. a.u., arbitrary units.

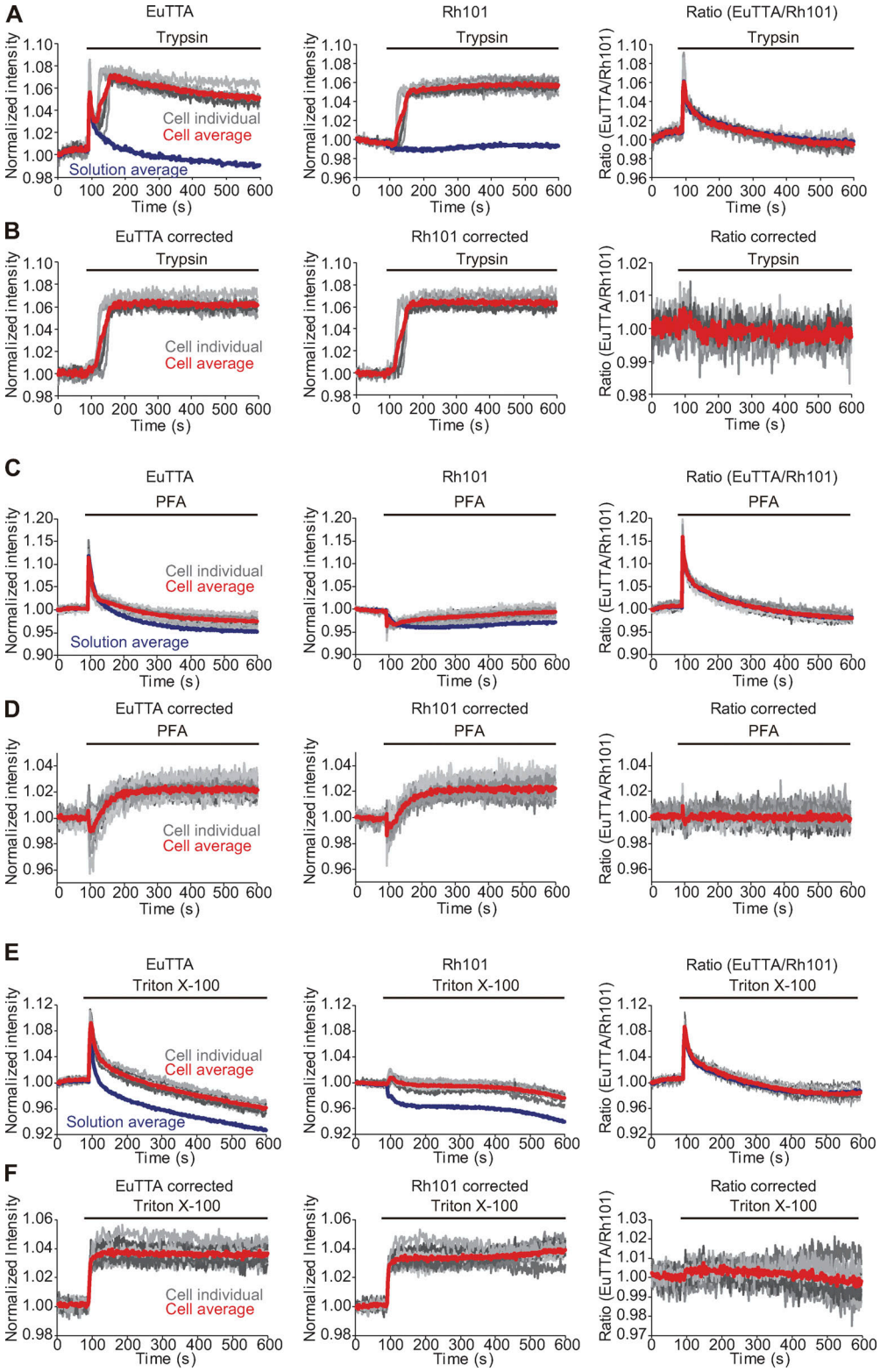

Figure S7. **Changes in the F.I. of RT nanosheets with HeLa cells before and after treatment with trypsin, PFA, or Triton X-100. (A)** Time course of changes in the F.I. of EuTTA (left), Rh101 (middle), and the EuTTA/Rh101 ratio of RT nanosheets upon trypsin (final 0.12%) treatment. Gray lines, individual cells; red lines, average of individual cells; blue lines, average without cells. **(B)** Same as in A with the F.I. corrected by that without cells. See Materials and methods for details. Gray lines, individual cells; red lines, average of individual cells. In A and B, the horizontal black line indicates the period for trypsin treatment. Number of cells, 12 (n = 3). **(C)** Same as in A upon PFA (final 4%) treatment. **(D)** Same as in C with the F.I. corrected by that without cells. In C and D, the horizontal black line indicates the period of PFA treatment. Number of cells, 21 (n = 3). **(E)** Same as in A upon Triton X-100 (final 0.9%) treatment for fixed HeLa cells with PFA. **(F)** Same as in E with the F.I. corrected by that without cells. In E and F, the horizontal black line indicates the period of Triton X-100 treatment. Number of cells, 14 (n = 3).

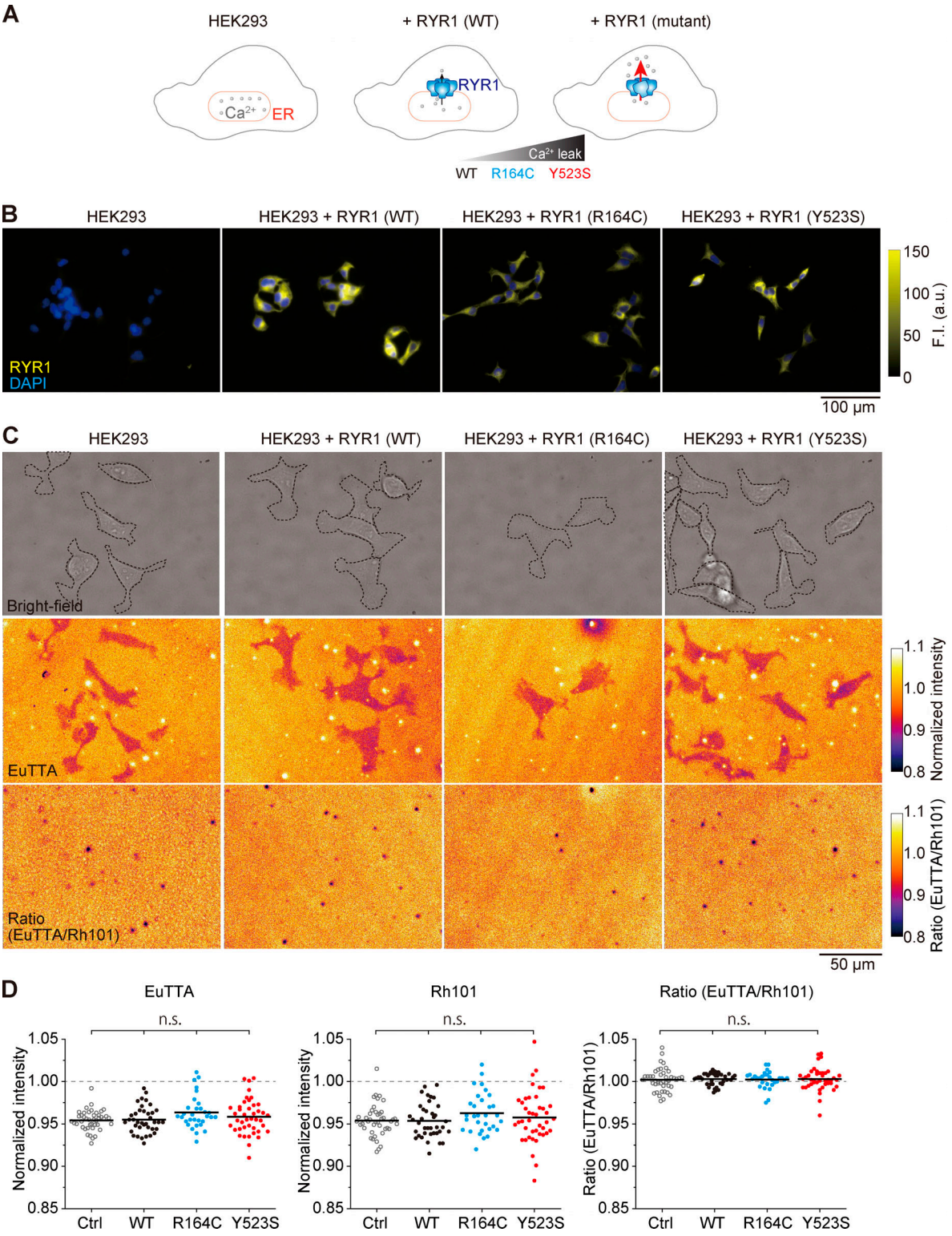

Figure S8. **Temperature measurement for HEK293 cells expressing malignant hyperthermia-causing RYR1 mutants. (A)** Illustration showing that the expression of mutant RYR1 in HEK293 cells causing the leak of Ca^{2+} from the ER. The magnitude of Ca^{2+} leak is greater for Y523S than R164C (Murayama et al., 2015). **(B)** Fluorescence images of HEK293 cells on RT nanosheets with or without RYR1 expression. RYR1 was visualized by immunostaining. From left to right: control HEK293 cells, HEK293 cells expressing WT RYR1, HEK293 cells expressing RYR1 (R164C), and HEK293 cells expressing RYR1 (Y523S). **(C)** Top: Bright-field images of various types of HEK293 cells on RT nanosheets. Middle: Normalized EuTTA fluorescence images of RT nanosheets (see Fig. S6). Bottom: EuTTA/Rh101 images of RT nanosheets. From left to right: control HEK293 cells, HEK293 cells expressing WT RYR1, HEK293 cells expressing RYR1 (R164C), and HEK293 cells expressing RYR1 (Y523S). **(D)** Comparison of normalized F.I. for EuTTA (left), Rh101 (middle), and the EuTTA/Rh101 ratio (right) on RT nanosheets. Number of cells, 43, 38, 31, and 42 for control (Ctrl) HEK293 cells, HEK293 cells expressing WT RYR1, RYR1 (R164C), and RYR1 (Y523S), respectively. The Steel–Dwass test was performed. a.u., arbitrary units; n.s., not significant.

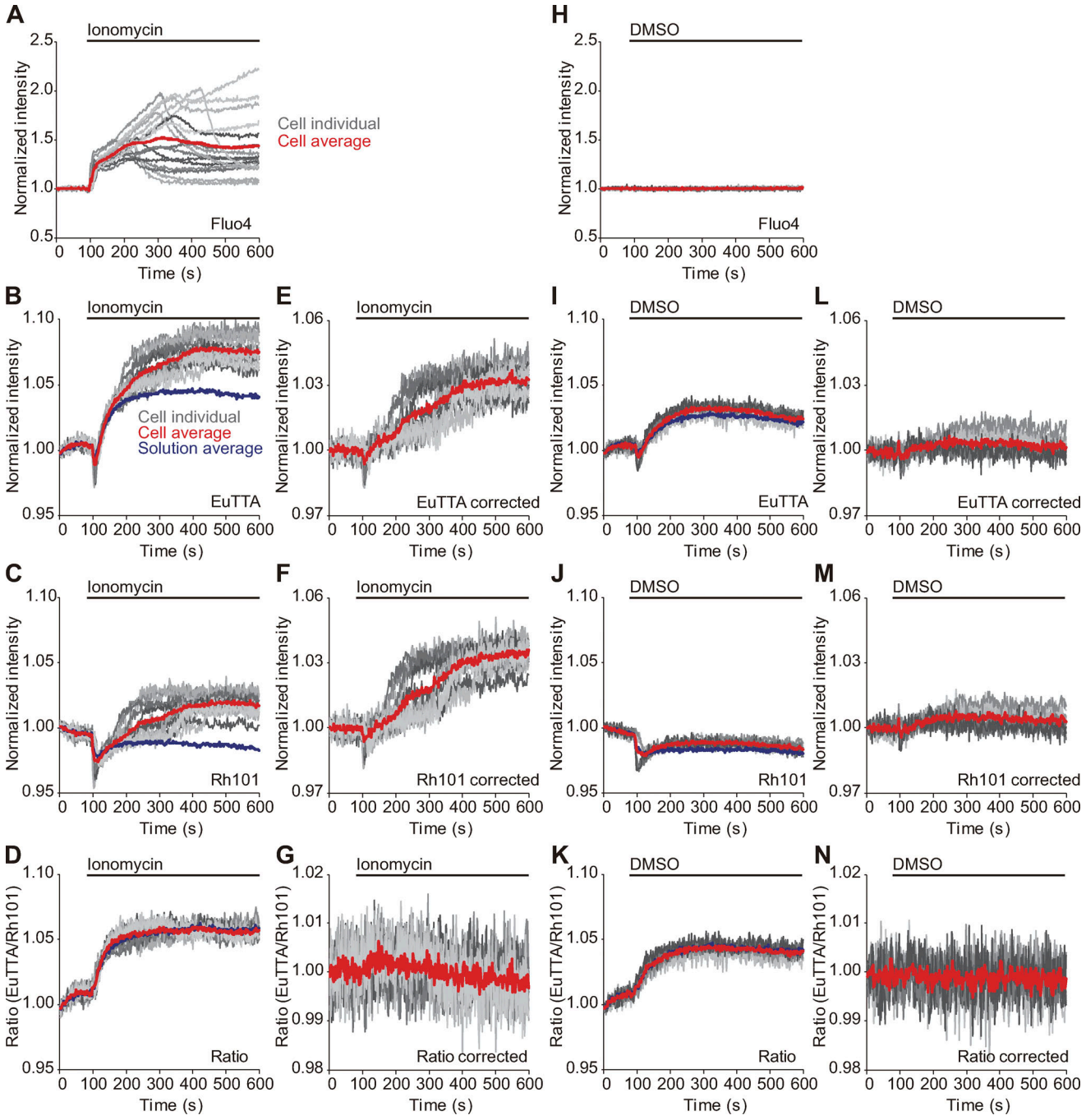

Figure S9. **Temperature measurement for HeLa cells on RT nanosheets upon ionomycin treatment. (A)** Time course of changes in Fluo4 F.I. in HeLa cells on RT nanosheets. Gray lines, individual cells; red line, average. Number of cells, 16 (n = 3). **(B)** Time course of changes in EuTTA F.I. **(C and D)** Same as in B for the F.I. of Rh101 and the EuTTA/Rh101 F.I. ratio, respectively. Gray lines, F.I. of RT nanosheets in individual cells; red line, average F.I.; blue line; average F.I. of RT nanosheets without cells. Number of cells, 16 (n = 3). **(E)** Time course of changes in the corrected EuTTA F.I. **(F and G)** Same as in E for the F.I. of Rh101 and the EuTTA/Rh101 F.I. ratio, respectively. Gray lines, F.I. of RT nanosheets in individual cells; red line, average F.I. F.I. was corrected by that of RT nanosheets without cells. See Materials and methods for details. In each graph, the horizontal black line indicates the period of ionomycin treatment (2 μM, 0.1% DMSO). **(H–N)** Same as in A–G, respectively, but with 0.1% DMSO (no ionomycin). Number of cells, 10 (n = 2).

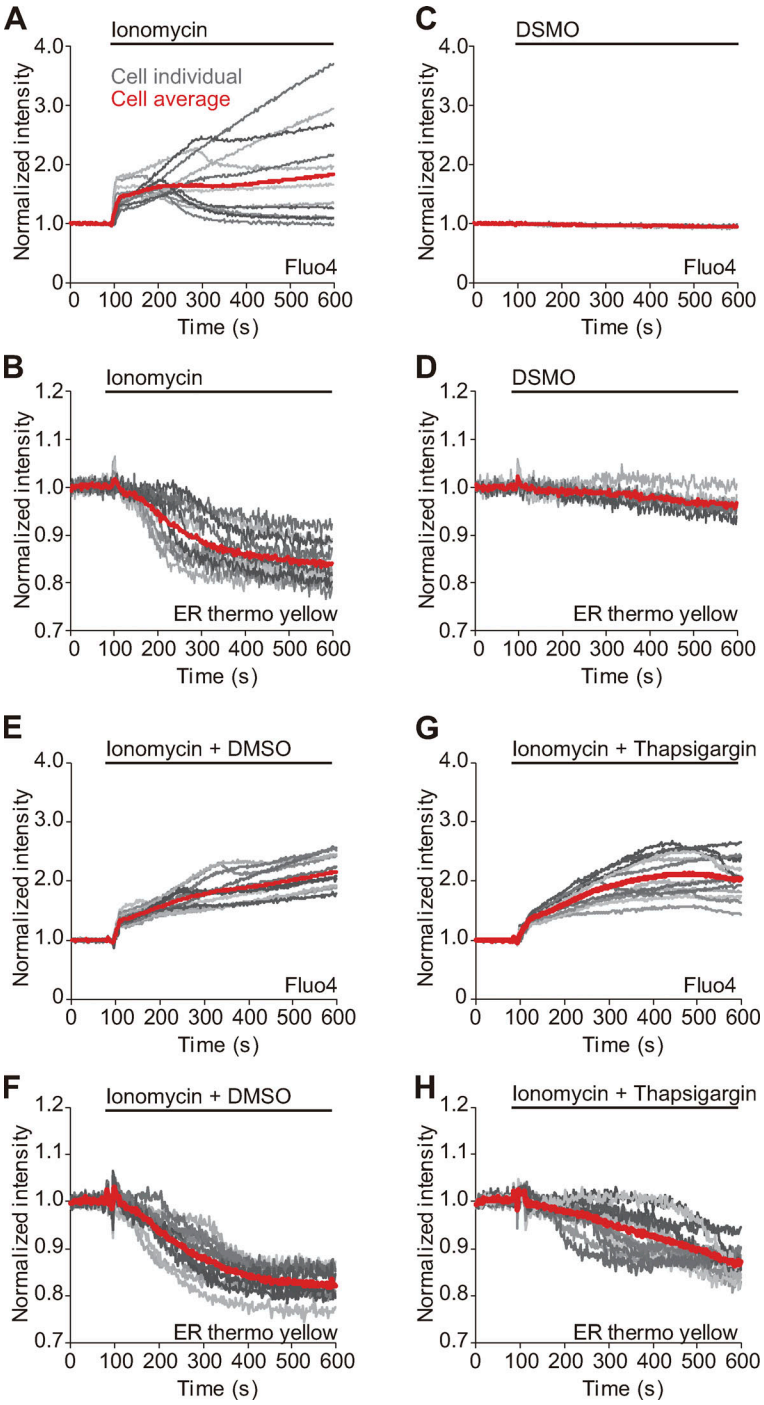

Figure S10. **Temperature measurement for the ER in HeLa cells on EuTTA nanosheets upon ionomycin treatment. (A)** Time course of changes in Fluo4 F.I. **(B)** Same as in A for ER thermo yellow F.I. Gray lines, data in individual cells; red line, averaged data. Number of cells, 12 (n = 3). In each graph, a horizontal black line indicates the period of ionomycin treatment (2 µM, 0.1% DMSO). **(C and D)** Same as in A and B, respectively, but with 0.1% DMSO (no ionomycin). Number of cells, 8 (n = 2). **(E and F)** Same as in A and B, respectively, but both ionomycin (2 µM, 0.1% DMSO) and 0.1% DMSO were added (total 0.2% DMSO). See Materials and methods for the details. Number of cells, 12 (n = 3). **(G and H)** Same as in A and B, respectively, but both ionomycin (2 µM, 0.1% DMSO) and thapsigargin (2 µM, 0.1% DMSO) were added (total 0.2% DMSO). Number of cells, 13 (n = 3).

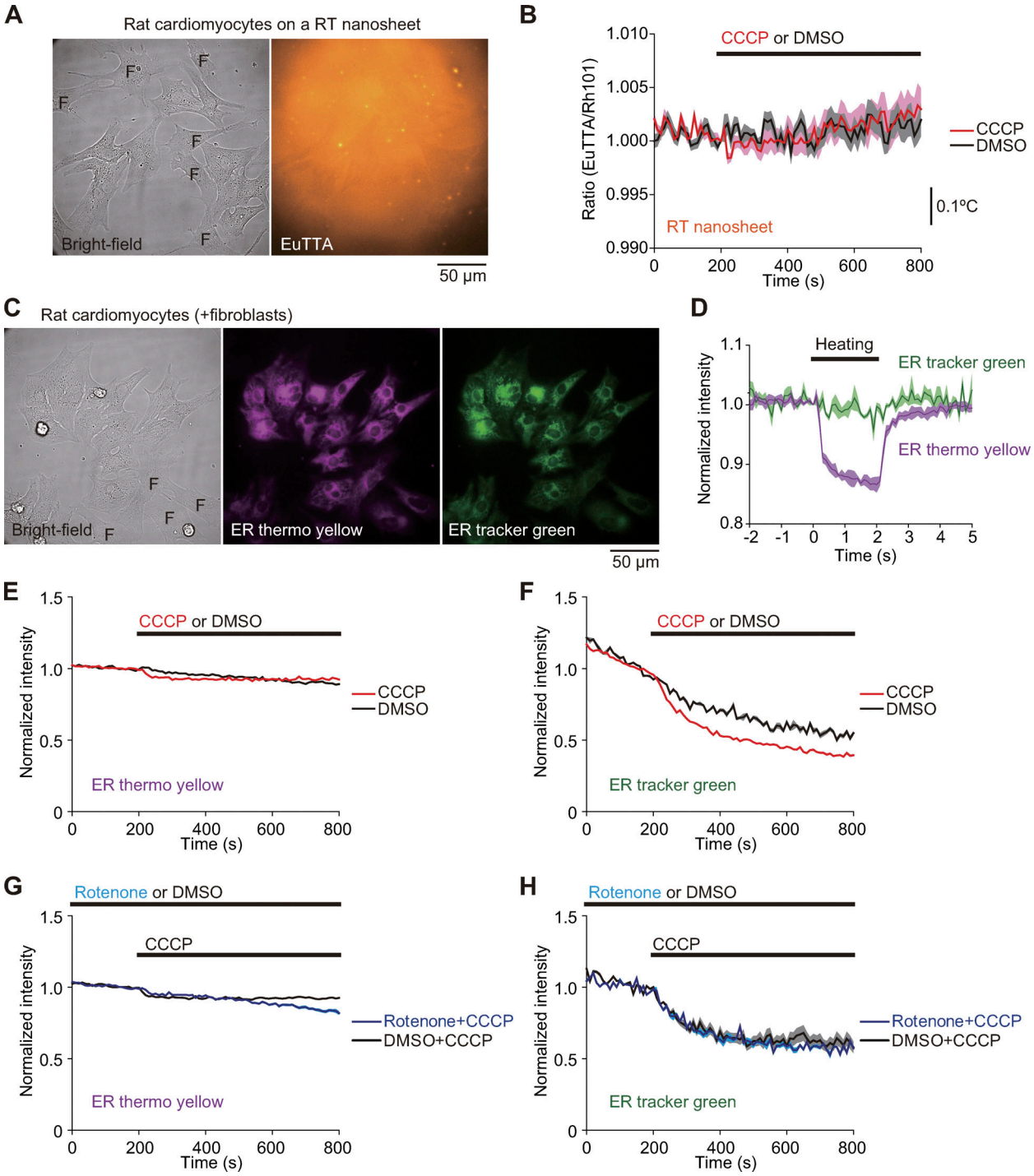

Figure S11. **Measurement for CCCP-induced thermogenesis in rat neonatal cardiomyocytes. (A)** Left: Bright-field image of rat neonatal cardiomyocytes and contaminating fibroblasts (indicated by "F"). Right: Fluorescence image of EuTTA for the cells on the left on a RT nanosheet. **(B)** Time course of changes in the EuTTA/Rh101 ratio of RT nanosheets with cardiomyocytes upon application of 10 µM CCCP (red) or 0.1% DMSO (black). Values were corrected by those obtained in the medium (see Materials and methods for details). Number of cells, 18 (n = 3) for both CCCP and DMSO. The horizontal black line indicates the period during which CCCP or DMSO was present. Calibration bar was calculated from the temperature sensitivity of RT nanosheets (−3.35%/°C, cf. Fig. 1 D). Data shown as mean ± SEM **(C)** Left: Bright-field image of rat neonatal cardiomyocytes and contaminating fibroblasts (indicated by "F") on a glass-bottom dish. Middle and right: Fluorescence images of ER thermo yellow and ER tracker green for the cells on left, respectively. **(D)** Time course of change in the F.I. of ER thermo yellow (purple) and ER tracker green (green) upon an increase in temperature by IR laser irradiation for 2 s (as indicated by "Heating"). F.I. around the heated center (9,331 µm^2) was measured. Data shown as mean ± SEM (n = 4). **(E)** Time course of changes in the F.I. of ER thermo yellow in cardiomyocytes before and after application of 10 µM CCCP (red) or 0.1% DMSO (black). **(F)** Same as in E for ER tracker green. In E and F, number of cells, 13 (n = 2) and 8 (n = 2) for CCCP and DMSO, respectively. Data shown as mean ± SEM. **(G)** Time courses of changes in the F.I. of ER thermo yellow in cardiomyocytes preincubated with 10 µM rotenone (blue) or 0.1% DMSO (black) for 30 min and then stimulated by 10 µM CCCP. **(H)** Same as in G for ER tracker green. In G and H, number of cells, 11 (n = 2) for both rotenone and DMSO. Data shown as mean ± SEM.

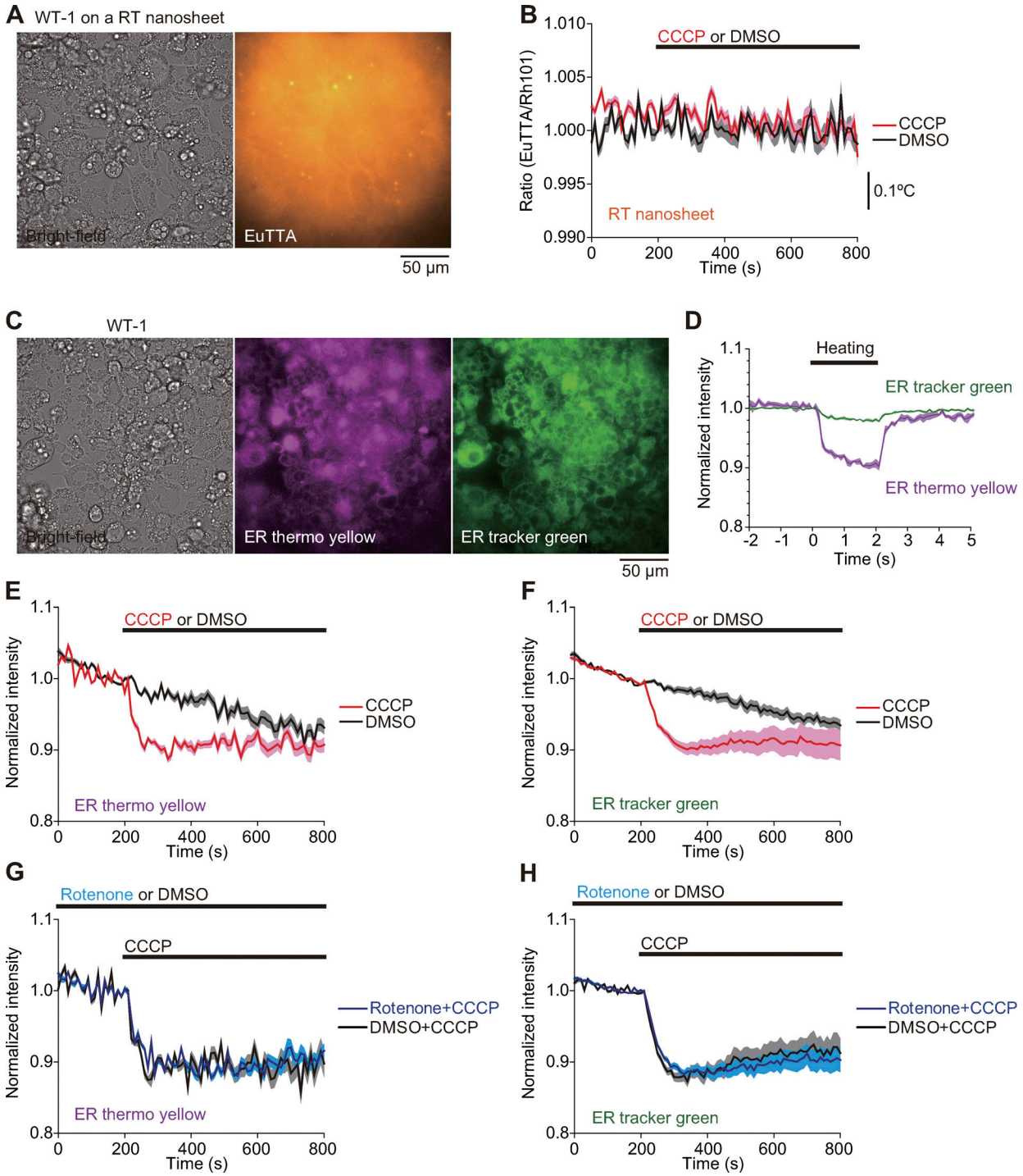

Figure S12. **Measurement for CCCP-induced thermogenesis in brown adipocytes derived from WT-1 cells. (A)** Left: Bright-field image of WT-1 adipocytes. Right: Fluorescence image of EuTTA of for the cells on a RT nanosheet. **(B)** Time course of changes in the EuTTA/Rh101 ratio of RT nanosheets with WT-1 adipocytes upon application of 10 µM CCCP (red) or 0.1% DMSO (black). Values were corrected by those obtained in the medium (see Materials and methods for details). Number of cells, 53 (n = 6) and 38 (n = 5) for CCCP and DMSO, respectively. The horizontal black line indicates the period during which CCCP or DMSO was present. Calibration bar was calculated from the temperature sensitivity of RT nanosheets (−3.35%/°C, cf. Fig. 1 D). Data shown as mean ± SEM. **(C)** Left: Bright-field image of WT-1 adipocytes on a glass-bottom dish. Middle and right: Fluorescence images of ER thermo yellow and ER tracker green for the cells on left, respectively. **(D)** Time course of changes in the F.I. of ER thermo yellow (purple) and ER tracker green (green) upon an increase in temperature by IR laser irradiation for 2 s (as indicated by "Heating"). F.I. around the heat center (9,331 µm^2) was measured. Data shown as mean ± SEM (n = 4). **(E)** Time courses of changes in the F.I. of ER thermo yellow in WT-1 adipocytes before and after application of 10 µM CCCP (red) or 0.1% DMSO (black). **(F)** Same as in E for ER tracker green. In E and F, number of cells, 37 (n = 4) and 43 (n = 4) for CCCP and DMSO, respectively. Data shown as mean ± SEM. **(G)** Time courses of changes in the F.I. of ER thermo yellow in WT-1 adipocytes preincubated with 10 µM rotenone (blue) or 0.1% DMSO (black) for 30 min and then stimulated by 10 µM CCCP. **(H)** Same as in G for ER tracker green. In G and H, number of cells, 38 (n = 5) and 29 (n = 3) for rotenone and DMSO, respectively. Data shown as mean ± SEM.

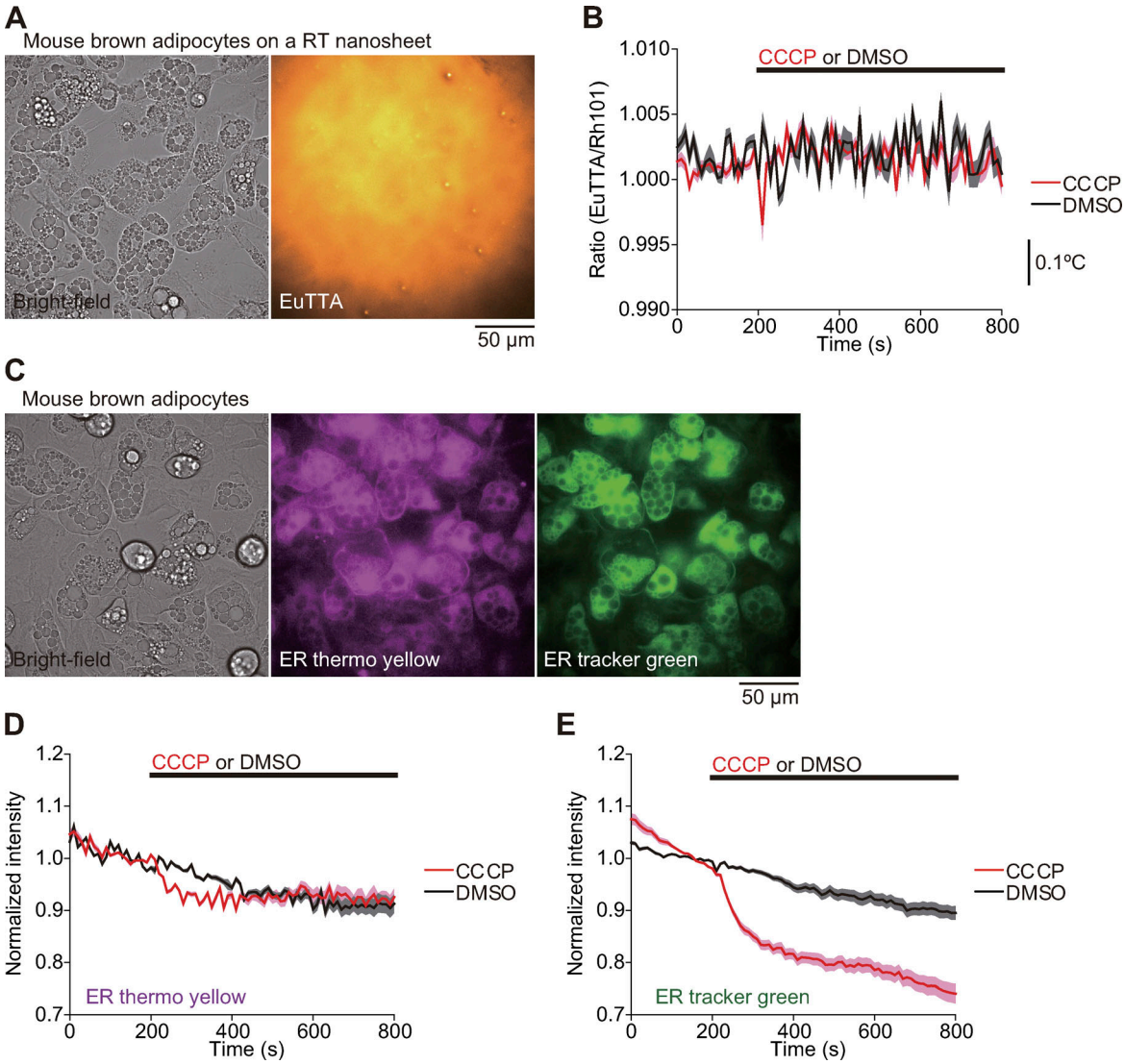

Figure S13. **Measurement for CCCP-induced thermogenesis in mouse brown adipocytes. (A)** Left: Bright-field image of mouse brown adipocytes. Right: Fluorescence image of EuTTA for the cells on a RT nanosheet. **(B)** Time course of changes in the EuTTA/Rh101 ratio of RT nanosheets with mouse brown adipocytes upon application of 10 µM CCCP (red) or 0.1% DMSO (black). Values were corrected by those obtained in the medium (see Materials and methods for details). Number of cells, 59 (n = 6) and 31 (n = 3) for CCCP and DMSO, respectively. The horizontal black line indicates the period during which CCCP or DMSO was present. Calibration bar was calculated from the temperature sensitivity of RT nanosheets (−3.35%/°C, cf. Fig. 1 D). Data shown as mean ± SEM. **(C)** Left: Bright-field image of mouse brown adipocytes on a glass-bottom dish. Middle and right: Fluorescence images of ER thermo yellow and ER tracker green for the cells on left, respectively. **(D)** Time course of changes in the F.I. of ER thermo yellow in mouse brown adipocytes before and after application of 10 µM CCCP (red) or 0.1% DMSO (black). **(E)** Same as in D for ER tracker green. In D and E, number of cells, 27 (n = 3) and 22 (n = 2) for CCCP and DMSO, respectively. Data shown as mean ± SEM.

Video 1. **Trypsin treatment for HeLa cells cultured on an EuTTA nanosheet.** Fluorescence image sequences of Calcein in cells (left) and of an EuTTA nanosheet (right). Trypsin (final concentration, 0.12%) was added at 90 s. Scale bar, 25 µm. See Fig. S1 A.

Video 2. **Skinning treatment for fixed HeLa cells cultured on an EuTTA nanosheet.** Fluorescence image sequences of CellMask Orange (left; i.e., cellular membranes), Calcein (middle), and an EuTTA nanosheet (right). Triton X-100 (final concentration: 0.9%) was added at 90 s. Scale bar, 25 µm. See Fig. S1 H.

Video 3. **Time-lapse image sequence of HeLa cells cultured on a RT nanosheet.** Scale bar, 100 µm. See Fig. S5 A.

Video 4. **Ionomycin treatment for HeLa cells cultured on a RT nanosheet.** Fluorescence image sequences of Fluo4 in the cells and EuTTA of a RT nanosheet. Ionomycin (final concentration, 2 µM) was added at 90 s. Scale bar, 25 µm. See also Fig. 3 A.

Video 5. **Ionomycin treatment for HeLa cells stained with ER thermo yellow cultured on an EuTTA nanosheet.** Fluorescence image sequences of Fluo4 and ER thermo yellow in the cells. Ionomycin (final concentration, 2 µM) was added at 90 s. Scale bar, 25 µm. See Fig. 3 D.

Video 6. **Ca^{2+} imaging of beating cardiomyocytes cultured on a RT nanosheet.** Fluorescence image sequence of Fluo4 in neonatal rat cardiomyocytes on the nanosheet. Electrical stimulation at 2 Hz was given at 0 s. Scale bar, 25 µm. See Fig. 4 A.

Video 7. **Bright-field image sequence of beating cardiomyocytes cultured on a RT nanosheet.** Electrical stimulation at 2 Hz was given at 0 s. Scale bar, 25 µm. See Fig. 4 A.

Video 8. **Ca^{2+} imaging of exciting neurons cultured on an EuTTA nanosheet.** Fluorescence image sequence of Fluo4 in rat hippocampal neurons on the nanosheet. Electrical stimulation at 0.25 Hz was given at 0 s. Scale bar, 25 µm. See Fig. 5 A.